Journal of Sound and Vibration (2000) **238**(1), 113–145
doi:10.1006/jsvi.2000.3152, available online at http://www.idealibrary.com on IDEAL®

HAMILTON'S PRINCIPLE FOR EXTERNAL VISCOUS FLUID–STRUCTURE INTERACTION

H. Benaroya and T. Wei

Department of Mechanical and Aerospace Engineering, Rutgers University, 98 Brett Road, Piscataway, NJ 08854, U.S.A.

(*Received* 8 *November* 1999, *and in final form* 8 *June* 2000)

Hamilton's principle is extended so as to be able to model external flow–structure interaction. This is accomplished by using Reynold's Transport theorem. In this form, Hamilton's principle is hybrid in the sense that it has an analytical part as well as a part that depends on experimentally derived functions. Examples are presented. The discussion on implications and extensions is extensive. In this work, a general theory is developed for the case where the configuration is *not* prescribed at the end times of the variational principle. This leads to a single governing equation of motion. This limitation can be removed by prescribing the end times, as usually done. This is outlined in the present paper, and will be the subject of a future paper.

A detailed discussion is also presented of the experimental work performed in parallel with and in support of the theoretical developments. As a true fluid-structural model, it is necessary to fully couple the dynamics. This has been the foundation of our formulation.

1. INTRODUCTION

One of the great challenges in engineering science also happens to be one of engineering design. This is the modelling, analysis and design of vibrating structures driven by fluid motion. Our particular concern here is the vortex-induced oscillations of a bluff body. While the importance of the subject has long been known, it is only during the past almost 30 years that there have been concerted efforts to analytically model the general behavior of the coupling between vortex shedding and structural oscillation. One may view the efforts of Hartlen and Currie [1] as initiating the flow-oscillator phase of modern research in this discipline.

In parallel, and over a longer period of time, experimentalists have been performing experiments and gathering data of such interactions in order to help define the various regimes of behavior as a function, for example, of flow velocity. There are numerous review papers [2–7] and journals devoted to this subject. The literature in fluid–structure interaction is vast, and it can be said to comprise a large fraction of all papers published in the mechanical sciences. Some representative papers are listed [8–31] to provide the reader with a sample of the various studies. The above-listed review papers would be an excellent starting point for the interested worker.

In this paper we are studying an approach that has been only barely noticed and for which the literature is essentially non-existent except for the initial work referred to next.

Hamilton's principle in analytical dynamics is certainly among the great intellectual achievements since the work of Newton. This variational principle, while developed as part of the evolution of our understanding of elastic body dynamics, has been applied in many

0022-460X/00/460113 + 33 $35.00/0

disciplines, including optics and quantum mechanics. In section 2, for completeness and to establish the notation used here, we will derive the principle, and then in section 3 show how it has been extended in the fundamental work of McIver [32] for systems of changing mass. In particular, the development by McIver was a successful attempt to model structures with internal moving fluid. We will build on this idea to extend Hamilton's principle for structures vibrating in a fluid. Our purpose, in addition to being fascinated by the variational principles of mechanics, is to use such an approach to semi-analytically model vortex-induced vibration. The "semi" implies that part of the model depends on experimental data. As we will show, there is no way that such a modelling effort can be accomplished without a close linkage to data derived in physical experiments and the input of the experimentalist. Experimental data not only helps us to verify the model predictions but also allows us to develop the most advantageous model framework from the variational mechanics perspective, as we will discuss in section 4.

The basic theory of section 4 is applied to simple examples in section 5. This leads to sections 6 and 7 where the experimental foundations of the concurrent effort are introduced and detailed for the reader. Experimental results are presented and discussed for one of the simple examples of section 5. Section 8 introduces an extension of the theory for more general formulations.

2. HAMILTON'S PRINCIPLE

2.1. THE CLASSICAL THEORY

From d'Alembert's principle for a system of n particles,

$$\sum_{i=1}^{n} \left(m_i \frac{\mathrm{d}^2 \mathbf{r}_i}{\mathrm{d}t^2} + \frac{\partial \Pi}{\partial \mathbf{r}_i} - \mathbf{F}_i \right) \cdot \delta \mathbf{r}_i = 0. \tag{1}$$

where $\Pi = \Pi(\mathbf{r}_1, \mathbf{r}_2, \ldots, \mathbf{r}_n)$ is the potential energy of the particles, $\mathbf{F}_i$ denotes forces without potentials acting on the ith particle, $\mathbf{r}_i$ is the position vector of the particle of mass m_i and $\delta \mathbf{r}_i$ is a virtual displacement. The notation δ implies a variation in a function. It is an imaginary alternative configuration that complies with the system constraints. The variation equals zero where the system is prescribed. For example, at a fixed boundary or support, the variation is zero since there cannot be any work done in this case. Also, if the configuration is prescribed, then the variation equals zero because otherwise there would result a configuration that is not possible. Considering each term in equation (1), we note that

$$\delta \Pi = \sum_{i=1}^{n} \left(\frac{\partial \Pi}{\partial \mathbf{r}_i} \right) \cdot \delta \mathbf{r}_i, \quad \delta W = \sum_{i=1}^{n} (\mathbf{F}_i) \cdot \delta \mathbf{r}_i \tag{2, 3}$$

and (by the product rule of differentiation)

$$\sum_{i=1}^{n} \left(m_i \frac{\mathrm{d}^2 \mathbf{r}_i}{\mathrm{d}t^2} \right) \cdot \delta \mathbf{r}_i = \frac{\mathrm{d}}{\mathrm{d}t} \left[\sum_{i=1}^{n} \left(m_i \frac{\mathrm{d}\mathbf{r}_i}{\mathrm{d}t} \right) \cdot \delta \mathbf{r}_i \right] - \sum_{i=1}^{n} \left(m_i \frac{\mathrm{d}\mathbf{r}_i}{\mathrm{d}t} \right) \cdot \delta \frac{\mathrm{d}\mathbf{r}_i}{\mathrm{d}t} \tag{4}$$

$$= \frac{\mathrm{d}}{\mathrm{d}t} \left[\sum_{i=1}^{n} \left(m_i \frac{\mathrm{d}\mathbf{r}_i}{\mathrm{d}t} \right) \cdot \delta \mathbf{r}_i \right] - \delta T, \tag{5}$$

where T is called the kinetic energy of the particles. On substituting equations (2), (3) and (5) into equation (1), d'Alembert's principle becomes

$$\delta \mathscr{L} + \delta W - \frac{\mathrm{d}}{\mathrm{d}t}\left[\sum_{i=1}^{n}\left(m_i \frac{\mathrm{d}\mathbf{r}_i}{\mathrm{d}t}\right)\cdot \delta \mathbf{r}_i\right] = 0, \tag{6}$$

where $\mathscr{L} = T - \Pi$ is known as the Lagrangian of the system. Equation (6) for a discrete system may be written for a continuous system as

$$\delta \mathscr{L} + \delta W - \frac{\mathrm{d}}{\mathrm{d}t}\left[\int_v (\rho \mathbf{U})\cdot \delta \mathbf{r}\, \mathrm{d}v\right] = 0, \tag{7}$$

where ρ denotes the density, $\mathbf{U} = \mathrm{d}\mathbf{r}/\mathrm{d}t$, the velocity field of the system at time t, $\mathscr{L}$ is the Lagrangian of the continuous system, and δW is the virtual work performed on the system by the generalized (non-conservative) forces undergoing virtual displacements. v denotes a fixed material system enclosed in a volume, over which the integration is performed.

Hamilton's principle is obtained by integrating equation (7) (or equation (6)) with respect to time over an interval t_1 to t_2, yielding

$$\delta \int_{t_1}^{t_2} \mathscr{L}\, \mathrm{d}t + \int_{t_1}^{t_2} \delta W\, \mathrm{d}t - \left[\int_v (\rho \mathbf{U})\cdot \delta \mathbf{r}\, \mathrm{d}v\right]_{t_1}^{t_2} = 0. \tag{8}$$

If one imposes the requirement that at times t_1 and t_2 the configuration be prescribed, then it must be that $\delta \mathbf{r} = 0$, and then the last term in the above equation drops out, leaving only

$$\delta \int_{t_1}^{t_2} \mathscr{L}\, \mathrm{d}t + \int_{t_1}^{t_2} \delta W\, \mathrm{d}t = 0. \tag{9}$$

The equations of motion and their respective boundary conditions are a result of performing the stated variations.

In this case, where the configuration is prescribed at the end times, Hamilton's principle states that there is an optimal (minimum) path in time for the configuration of the system. This is not generally the case where the end times are not prescribed, as we will see in our subsequent discussion. It is important to emphasize the physical meaning of prescribing the configuration and how this leads to a variational principle to which there is an optimal configuration in dynamic space. Prescribing the variation $\delta \mathbf{r}$ at the end times implies that the system configuration is known at those times, thus leading to $\delta \mathbf{r} = \mathbf{0}$, and then it is therefore possible to meaningfully speak of an optimal path between the end times.

2.2. A GENERALIZATION

If we cannot state that the variation is between definite limits t_1 and t_2, then there may be a variation as well at the ends of the time interval. The implication is that the system is not prescribed at these end times. Equation (9) was obtained assuming no such variation. Begin

with equation (6) and integrate between t_1 and t_2. Then,

$$\delta \int_{t_1}^{t_2} \mathscr{L}\, \mathrm{d}t + \int_{t_1}^{t_2} \delta W\, \mathrm{d}t - \int_{t_1}^{t_2} \frac{\mathrm{d}}{\mathrm{d}t}\left[\sum_{i=1}^{n}\left(m_i \frac{\mathrm{d}\mathbf{r}_i}{\mathrm{d}t}\right)\cdot \delta \mathbf{r}_i\right] \mathrm{d}t = 0,$$

$$\delta \int_{t_1}^{t_2} \mathscr{L}\, \mathrm{d}t + \int_{t_1}^{t_2} \delta W\, \mathrm{d}t = \left[\sum_{i=1}^{n}\left(m_i \frac{\mathrm{d}\mathbf{r}_i}{\mathrm{d}t}\right)\cdot \delta \mathbf{r}_i\right]_{t_1}^{t_2}. \tag{10}$$

Following Lanczos [33], let the virtual displacement $\delta\mathbf{r}_i$ at each instant of time coincide with the actual displacement $\mathrm{d}\mathbf{r}_i$ which takes place during an infinitesimal time $\mathrm{d}t \equiv \varepsilon$. Then $\delta\mathbf{r}_i = \mathrm{d}\mathbf{r}_i = \varepsilon\dot{\mathbf{r}}_i$ and

$$\left[\sum_{i=1}^{n}\left(m_i \frac{\mathrm{d}\mathbf{r}_i}{\mathrm{d}t}\right)\cdot \delta \mathbf{r}_i\right]_{t_1}^{t_2} = \left[\sum_{i=1}^{n}(m_i\dot{\mathbf{r}}_i)\cdot \varepsilon\dot{\mathbf{r}}_i\right]_{t_1}^{t_2} = \left[\sum_{i=1}^{n} \varepsilon m_i \dot{r}_i^2\right]_{t_1}^{t_2},$$

where, as an aside, it is noted that $m_i\dot{r}_i^2 \equiv p_i\dot{r}_i$ and p_i is the momentum of particle i. Furthermore,

$$\delta \int_{t_1}^{t_2} \mathscr{L}\, \mathrm{d}t = \int_{t_1}^{t_2} \mathrm{d}\mathscr{L}\, \mathrm{d}t = \int_{t_1}^{t_2} \varepsilon\dot{\mathscr{L}}\, \mathrm{d}t = [\varepsilon\mathscr{L}]_{t_1}^{t_2},$$

$$\int_{t_1}^{t_2} \delta W\, \mathrm{d}t = \int_{t_1}^{t_2} \mathrm{d}W\, \mathrm{d}t = \int_{t_1}^{t_2} \varepsilon\dot{W}\, \mathrm{d}t = [\varepsilon W]_{t_1}^{t_2}.$$

Equation (10) can now be written as

$$[\varepsilon\mathscr{L}]_{t_1}^{t_2} + [\varepsilon W]_{t_1}^{t_2} = \left[\sum_{i=1}^{n} \varepsilon m_i \dot{r}_i^2\right]_{t_1}^{t_2},$$

or, substituting the expression for p_i and eliminating ε,

$$\left[\sum_{i=1}^{n} p_i\dot{r}_i - \mathscr{L}\right]_{t_1}^{t_2} = [W]_{t_1}^{t_2}. \tag{11}$$

In equation (11), the right-hand side represents the non-conservative work done on the system and the left-hand side represents the total energy in the system. We know that $\mathscr{L} = T - \Pi$, where T is a quadratic in the velocities $\dot{r}_i$,

$$T = \frac{1}{2}\sum_{i,k=1}^{n} a_{ik}\dot{r}_i\dot{r}_k,$$

where a_{ik} are not functions of $\dot{r}_i$, and Π is ordinarily independent of velocity. Therefore,

$$p_i = \frac{\partial T}{\partial \dot{r}_i} = \sum_{k=1}^{n} a_{ik}\dot{r}_k$$

and

$$\sum_{i=1}^{n} p_i \dot{r}_i = \sum_{i,k=1}^{n} a_{ik} \dot{r}_i \dot{r}_k = 2T.$$

Therefore, equation (11) can be written as

$$[2T - (T - \Pi)]_{t_1}^{t_2} = [W]_{t_1}^{t_2}.$$

If there is no non-conservative work done on the system, then $[W]_{t_1}^{t_2} = 0$, and we have $T + \Pi = constant$, which is a statement of the principle of conservation of energy. In general, however, $\Delta(T + \Pi) = \Delta W$. Divide both sides by Δt and take the limit as $\Delta t \to 0$, then over the time span t_1 to t_2,

$$\frac{\mathrm{d}(T + \Pi)}{\mathrm{d}t} = \dot{W}; \tag{12}$$

that is, the total change in system energy is equal to the rate at which (non-conservative) work is done on the system. These developments can be extended to an open system, as shown in the following section, where we summarize some of the key results due to McIver.

3. McIVER'S EXTENSION OF HAMILTON'S PRINCIPLE

In 1973, McIver published a work with broad implications for modelling complex fluid–structure interactions. The central feature of his work was the broadening of Hamilton's principle to include integral control volume concepts from fluid mechanics. In this section, we summarize the key developments by McIver; however, adopting a notation that is consistent with our own developments that begin in section 4.

3.1. A BRIEF REVIEW OF REYNOLDS TRANSPORT THEOREM

Before proceeding with a discussion of McIver's extension, it would perhaps be instructive to briefly review Reynolds transport theorem. We first define a *system* as a collection of fluid particles comprising part of a flow of interest. The system boundaries are such that the same fluid elements are always contained therein. Necessarily, the mass of a system is constant, and it is in principle possible to write equations of motion for the system. For many flows, however, such a formulation would be intractable or inconvenient at best. For this reason, we define a *control volume* as a clearly defined, albeit imaginary, space through which fluid may pass. The external boundary of the control volume is referred to as the *control surface*. The advantage of this approach is that the boundaries of the control volume are prescribed at all times. Typically, one dictates that the control volume coincide with some physically meaningful boundary in the flow, e.g., the internal passage ways of a jet aircraft engine. In this context, it may be expedient to allow the control volume to move or change shape depending on the flow of interest.

Now suppose that at some time, t_0, a collection of fluid particles comprising a system occupies the same space as a control volume. It is possible to write the rate of change of any property of that system in terms of control volume parameters. This is the classic Reynolds

transport theorem which may be written as

$$\frac{\mathrm{d}}{\mathrm{d}t}\int_{system}(\mathscr{A}\rho)\,\mathrm{d}v = \int_{\substack{control\\vol}}\frac{\partial}{\partial t}(\mathscr{A}\rho)\,\mathrm{d}v - \int_{\substack{control\\surface}}(\mathscr{A}\rho)\mathbf{U}\cdot\mathbf{n}\,\mathrm{d}s. \tag{13}$$

In this form, $\mathscr{A}$ represents the property of interest per unit mass (intensive property), ρ is the fluid density, $\mathrm{d}v$ and $\mathrm{d}s$ are differential volumes and control surface area elements, respectively, and $\mathbf{U} = \mathbf{U}(\mathbf{x}, t)$ is the fluid velocity at any point on the control surface. Since $\rho(\mathbf{U}\cdot\mathbf{n})$ is the mass flow rate of fluid across a differential area element of the control surface, equation (13) may be physically interpreted as a balance equation for the property $\mathscr{A}$. Specifically, the rate of change of $\mathscr{A}$ contained within the system (i.e., the left-hand side of equation (13)) is equal to the rate of change of $\mathscr{A}$ within the control volume plus the net flux of $\mathscr{A}$ across the boundaries of the control volume. The unit normal $\mathbf{n}$ is defined as positive when pointing outward from a control surface. Therefore, for a flow into the control volume the sign of $\mathbf{U}\cdot\mathbf{n}$ is negative and for a flow out of the control volume the sign of $\mathbf{U}\cdot\mathbf{n}$ is positive. The control surface integral above is given a negative sign so that an increase in the system property $\mathscr{A}\rho$ with time occurs with a flow into the control volume.

Finally, it is important to note that $\mathbf{U}$ represents the fluid velocity relative to an inertial reference frame. Thus, if any part of the control surface is moving relative to such inertial frame, it becomes necessary to subtract the control surface velocity from the fluid velocity, $\mathbf{U} - \mathbf{V}_{control}$, to obtain the flow rate across the control volume boundaries. All quantities are defined or measured with respect to an observer at a fixed, or inertial control volume.

3.2. McIVER'S EXTENSION

The strength of McIver's work was in identifying an approach for analyzing complex interactions where the system boundaries are not necessarily well defined or where the system configuration at two distinct times may not be readily prescribed. In the classical Hamilton's principle approach, the system contains one or more solid objects whose positions may be prescribed at specific times. That is, the system is of fixed mass containing the same material elements at all times. By introducing Reynolds transport theorem, McIver generalized the analysis to include control volumes where the material is permitted to cross the boundaries. Specifically, by applying Reynolds transport theorem, equation (13), to the last term in equation (7), we obtain

$$\delta\mathscr{L}_{system} + \delta W - \int_{\substack{control\\vol}}\frac{\partial}{\partial t}(\rho\mathbf{U})\cdot\delta\mathbf{r}\,\mathrm{d}v + \int_{\substack{control\\surface}}(\rho\mathbf{U})\cdot\delta\mathbf{r}(\mathbf{U}-\mathbf{V}_{control})\cdot\mathbf{n}\,\mathrm{d}s = 0, \tag{14}$$

where, in the Lagrangian of the open control volume, $\mathscr{L}_{system}$, the mass is not fixed. We have retained the possibility of a moving control surface by including $\mathbf{V}_{control}$, which may have a different value in different regions of the control surface. The control surface here implies an open region since at closed portions flow velocity $\mathbf{U} = \mathbf{V}_{structure}$. Equation (14) is a statement of the principle of virtual work.

Now integrating with respect to time over the interval t_1 and t_2, and *again requiring the system configurations at t_1 and t_2 to be prescribed*, the extended form of Hamilton's principle for a system of changing mass can be expressed as

$$\delta\int_{t_1}^{t_2}\mathscr{L}_{system}\,\mathrm{d}t + \int_{t_1}^{t_2}\delta W\,\mathrm{d}t + \int_{t_1}^{t_2}\mathrm{d}t\int_{\substack{control\\surface}}(\rho\mathbf{U})\cdot\delta\mathbf{r}(\mathbf{U}-\mathbf{V}_{control})\cdot\mathbf{n}\,\mathrm{d}s = 0, \tag{15}$$

where δW is the virtual work performed by the non-potential forces acting on the same system. If the control surface (CS) does not move, then $\mathbf{V}_{control} = 0$. If only a portion of the control surface moves then the integral will be split into parts that follow the moving control surface and parts that are static. For the case where the virtual work arises from the surface tractions over the closed and open boundaries of the system, we have

$$\begin{aligned}\delta W &= \delta W_{closed\ CS} + \delta W_{open\ CS} \\ &= \int_{closed\ CS} (\boldsymbol{\sigma}\cdot\mathbf{n})\cdot\delta\mathbf{r}\,\mathrm{d}s + \int_{open\ CS} (\boldsymbol{\sigma}\cdot\mathbf{n})\cdot\delta\mathbf{r}\,\mathrm{d}s,\end{aligned} \tag{16}$$

where $\boldsymbol{\sigma}$ is the general stress tensor. Equation (15) then becomes

$$\begin{aligned}\delta\int_{t_1}^{t_2}\mathscr{L}_{system}\,\mathrm{d}t + \int_{t_1}^{t_2}\mathrm{d}t + \int_{open\ CS}[(\boldsymbol{\sigma}\cdot\mathbf{n})\cdot\delta\mathbf{r} + \rho\mathbf{U}\cdot\delta\mathbf{r}\,(\mathbf{U}-\mathbf{V}_{control})\cdot\mathbf{n}]\,\mathrm{d}s \\ + \int_{t_1}^{t_2}\mathrm{d}t\int_{closed\ CS}(\boldsymbol{\sigma}\cdot\mathbf{n})\cdot\delta\mathbf{r}\,\mathrm{d}s = 0.\end{aligned} \tag{17}$$

For a system that comprises a structure and a fluid, the above terms must account for both. Term $\mathscr{L}_{system}$ includes both structure and fluid, $\delta W_{open\ CS}$ represents open portions of the control surface through which fluid flows, and $\delta W_{closed\ CS}$ represents boundaries through which there is no flow, such as a solid boundary or a streamline.

McIver's system is composed of one control volume, part of which is open and the rest is closed. Therefore, both are treated simultaneously, as shown in the two examples developed in his paper. The first is the derivation of the equation of motion of a rocket where the open part of the control surface coincides with the exhaust for combusted fuel. The second example discusses an early controversy regarding the modelling of the dynamics of a moving beam.

3.3. SYSTEM CONFIGURATION NOT PRESCRIBED AT t_1 AND t_2

If the system configuration is not prescribed at the end times, we must proceed differently after equation (14). If *the system is not prescribed at* t_1 *and* t_2, the variation of the displacement $\delta\mathbf{r} \neq 0$, rather, we have the following[†] relation $\delta\mathbf{r} = \mathbf{U}\,\mathrm{d}t$. From this, we can see that the variational operator is related to the time differential operator by $\delta(\cdot) = \mathrm{d}t\,\mathrm{d}(\cdot)/\mathrm{d}t$. Begin with equation (14), repeated here,

$$\delta\mathscr{L}_{system} + \delta W - \int_{\substack{control\\vol}}\frac{\partial}{\partial t}(\rho\mathbf{U})\cdot\delta\mathbf{r}\,\mathrm{d}v + \int_{\substack{control\\surface}}(\rho\mathbf{U})\cdot\delta\mathbf{r}(\mathbf{U}-\mathbf{V}_{control})\cdot\mathbf{n}\,\mathrm{d}s = 0,$$

interchange the partial derivative with the integration over the control volume, and replace the variation as noted above,

$$\begin{aligned}\mathrm{d}t\,\frac{\mathrm{d}\mathscr{L}_{system}}{\mathrm{d}t} + \mathrm{d}t\,\frac{\mathrm{d}W}{\mathrm{d}t} - \int_{\substack{control\\vol}}\frac{\partial}{\partial t}(\rho\mathbf{U})\cdot\mathbf{U}\,\mathrm{d}t\,\mathrm{d}v \\ + \int_{\substack{control\\surface}}(\rho\mathbf{U})\cdot\mathbf{U}\,\mathrm{d}t\,(\mathbf{U}-\mathbf{V}_{control})\cdot\mathbf{n}\,\mathrm{d}s = 0.\end{aligned}$$

[†]As before, we replace the *arbitrary* variation $\delta\mathbf{r}$ by the actual $\mathrm{d}\mathbf{r} = \dot{\mathbf{r}}\,\mathrm{d}t$.

Eliminate the common $\mathrm{d}t$ factor to find

$$\frac{\mathrm{d}\mathscr{L}_{system}}{\mathrm{d}t} + \frac{\mathrm{d}W}{\mathrm{d}t} - \int_{\substack{control\\vol}} \frac{\partial}{\partial t}\rho U^2 \,\mathrm{d}v + \int_{\substack{control\\surface}} \rho U^2 (\mathbf{U} - \mathbf{V}_{control})\cdot \mathbf{n}\,\mathrm{d}s = 0. \tag{18}$$

For this system, we have

$$\mathscr{L}_{system} = \int_{system} \left(\frac{1}{2}\rho U^2\right)\mathrm{d}v - \int_{system} (\rho e)\,\mathrm{d}v = \int_{system} \left(\frac{1}{2}\rho U^2 - \rho e\right)\mathrm{d}v,$$

where e is the potential energy per unit mass. Now apply Reynolds transport theorem, equation (13), to $\mathscr{L}_{system}$,

$$\frac{\mathrm{d}}{\mathrm{d}t}\mathscr{L}_{system} = \frac{\mathrm{d}}{\mathrm{d}t}\int_{system}\left(\frac{1}{2}\rho U^2 - \rho e\right)\mathrm{d}v = \int_{\substack{control\\vol}} \frac{\partial}{\partial t}\left(\frac{1}{2}\rho U^2 - \rho e\right)\mathrm{d}v$$

$$- \int_{\substack{control\\surface}} \left(\frac{1}{2}\rho U^2 - \rho e\right)(\mathbf{U} - \mathbf{V}_{control})\cdot \mathbf{n}\,\mathrm{d}s.$$

Substitute this expression into equation (18) to find

$$\int_{\substack{control\\vol}} \frac{\partial}{\partial t}\left(\frac{1}{2}\rho U^2 - \rho e\right)\mathrm{d}v + \dot{W} - \frac{\mathrm{d}}{\mathrm{d}t}(2T)$$

$$+ \int_{\substack{control\\surface}} \rho\left[U^2 - \frac{1}{2}U^2 + e\right](\mathbf{U} - \mathbf{V}_{control})\cdot \mathbf{n}\,\mathrm{d}s = 0,$$

where

$$\int_{\substack{control\\vol}} \rho U^2\,\mathrm{d}v = 2T,$$

and T represents the kinetic energy of all the fluid within the control volume. Then,

$$\frac{\mathrm{d}(-T - \Pi)}{\mathrm{d}t} + \dot{W} + \int_{\substack{control\\surface}} \left[\frac{1}{2}\rho U^2 + \rho e\right](\mathbf{U} - \mathbf{V}_{control})\cdot \mathbf{n}\,\mathrm{d}s = 0.$$

Finally,

$$\frac{\mathrm{d}(T + \Pi)^{control}_{vol}}{\mathrm{d}t} = \dot{W} + \int_{\substack{control\\surface}} \rho\left[\frac{1}{2}U^2 + e\right](\mathbf{U} - \mathbf{V}_{control})\cdot \mathbf{n}\,\mathrm{d}s. \tag{19}$$

This equation states that the change in energy of a system equals the rate at which non-conservative work is done on the system plus the rate of gain of energy by virtue of the fluid flowing through the control surface and the advancing control surface engulfing particles. With the exception of the integral on the right-hand side, this equation is identical to equation (12).

4. THE EXTENSION FOR EXTERNAL VISCOUS FLOWS

McIver derived his extension for applications where the fluid is encased in the structure. The equations derived above assume a steady frictionless flow. The examples he studied include the rocket, and flow in a pipe. The application of interest here has the structure within the fluid. In particular, we are interested in generalizing the McIver extension of Hamilton's principle so that we can model the vortex-induced oscillation of a structure. This is a viscous external fluid–structure interaction. McIver's extension utilizes the control volume concept to account for fluid mass that enters and leaves the structure. This same idea can be applied to a control volume around a fluid that has a structure internally.

Modelling of the internal flow problem has the advantage that, assuming no cavitation, the fluid is bound by the structure. With external flows, the fluid is unbounded and the modelling becomes more challenging.

In this development it is useful to think of the system, comprising a structure surrounded by a moving fluid, as one that is defined using *two* control surfaces. The first control surface is at the structure surface. It is a closed control volume. The second control surface is at some distance from the structure, as shown in the figures below. This control surface may be partially closed and partially open, or all open, depending on the application. It is important to keep track of the various portions of the control surface so that the parameters are appropriately prescribed.

For such a control volume,

- there is a time rate change of momentum within the control volume due to the unsteady character of the flow,
- there is a net momentum flux across the boundaries of the control surface,
- there is an instantaneous pressure p acting on the control surface,
- there is an instantaneous shear stress τ acting on the control surface.

Begin with equation (14), repeated here,

$$\delta \mathscr{L}_{system} + \delta W - \int_{\substack{control \\ vol}} \frac{\partial}{\partial t}(\rho U)\cdot \delta \mathbf{r}\, \mathrm{d}v + \int_{\substack{control \\ surface}} (\rho \mathbf{U})\cdot \delta \mathbf{r}(\mathbf{U} - \mathbf{V}_{control})\cdot \mathbf{n}\cdot \mathrm{d}s = 0.$$

The integral over the control volume need to be interpreted here to include the inner (structural) as well as outer (fluid) control volumes.

Replace δW as follows,

$$\delta W = \int_{\substack{closed \\ CS}} (\boldsymbol{\sigma}\cdot \mathbf{n})\cdot \delta \mathbf{r}\, \mathrm{d}s + \int_{\substack{open \\ CS}} (\boldsymbol{\sigma}\cdot \mathbf{n})\cdot \delta \mathbf{r}\, \mathrm{d}s, \tag{20}$$

where $\mathbf{n}$ is an outward normal in the positive sense.

The integral over the closed surface represents the virtual work done by shear forces at the boundaries of the control volume where there is no flow across the control surface, for

example, at the cylinder wall, possibly other solid boundaries, or at streamlines. The integral over the open surface represents the virtual work done by normal and shear forces at the boundaries of the control volume where there is a flow across the control surface, for example, at the upstream and downstream surfaces, which may be perpendicular to the flow direction. The integrals above can be written more specifically as

$$\int_{\substack{closed\\CS}} (\boldsymbol{\sigma}\cdot\mathbf{n})\cdot\delta\mathbf{r}\,\mathrm{d}s = \int_{\substack{closed\\CS}} (-p\mathbf{n}+\tau_c)\cdot\delta\mathbf{r}\,\mathrm{d}s, \tag{21}$$

$$\int_{\substack{open\\CS}} (\boldsymbol{\sigma}\cdot\mathbf{n})\cdot\delta\mathbf{r}\,\mathrm{d}s = \int_{\substack{open\\CS}} (-p\mathbf{n}+\tau_o)\cdot\delta\mathbf{r}\,\mathrm{d}s, \tag{22}$$

where $-p\mathbf{n}$ is the normal pressure (inward) and $\boldsymbol{\tau}_c$ and $\boldsymbol{\tau}_o$ are the shear forces on the closed (structural) and open (fluid) surfaces of the control volume.

There are two ways to proceed. One can prescribe the configuration or not prescribe the configuration at the end times. We begin by not prescribing the configuration at the end times.

4.1. CONFIGURATION NOT PRESCRIBED AT t_1 AND t_2

We now follow the procedure of section 3 where the configuration is not prescribed at t_1 or t_2. We define $\delta\mathbf{r}$ as before, with the variational operator related to the time differential operator by $\delta(\cdot) = \mathrm{d}t\,\mathrm{d}(\cdot)/\mathrm{d}t$. Then,

$$\delta W = \int_{\substack{closed\\CS}} (-p\mathbf{n}+\boldsymbol{\tau}_c)\cdot\delta\mathbf{r}\,\mathrm{d}s + \int_{\substack{open\\CS}} (-p\mathbf{n}+\boldsymbol{\tau}_o)\cdot\delta\mathbf{r}\,\mathrm{d}s,$$

$$\mathrm{d}t\,\frac{\mathrm{d}W}{\mathrm{d}t} = \mathrm{d}t\int_{\substack{closed\\CS}} (-p\mathbf{n}+\boldsymbol{\tau}_c)\cdot\mathbf{U}\,\mathrm{d}s + \mathrm{d}t\int_{\substack{open\\CS}} (-p\mathbf{n}+\boldsymbol{\tau}_o)\cdot\mathbf{U}\,\mathrm{d}s,$$

where it is noted that the work done at the cylinder surface is independent of the control surface.

The integral over the control volume must be considered in the following way. For the inner control volume $\delta\mathbf{r} = \mathbf{U}_{structure}\,\mathrm{d}t$ and for the outer control volume (annulus) $\delta\mathbf{r} = \mathbf{U}\mathrm{d}t$, where $\mathbf{U}_{fluid} \equiv \mathbf{U}$. Therefore,

$$\frac{\partial}{\partial t}\int_{\substack{control\\vol}} (\rho\mathbf{U})\cdot\delta\mathbf{r}\,\mathrm{d}v = \frac{\partial}{\partial t}\int_{\substack{control\\vol}} [\rho U^2 + \rho_{structure}U^2_{structure}]\,\mathrm{d}v\,\mathrm{d}t.$$

Then, beginning with equation (18), repeated here, with $\rho \equiv \rho_{fluid}$,

$$\frac{\mathrm{d}\mathscr{L}_{system}}{\mathrm{d}t} + \frac{\mathrm{d}W}{\mathrm{d}t} - \frac{\partial}{\partial t}\int_{\substack{control\\vol}} [\rho U^2 + \rho_{structure}U^2_{structure}]\,\mathrm{d}v$$

$$+ \int_{\substack{control\\surface}} \rho U^2(\mathbf{U}-\mathbf{V}_{control})\cdot\mathbf{n}\,\mathrm{d}s = 0,$$

we find

$$\frac{\mathrm{d}}{\mathrm{d}t}\mathscr{L}_{system} + \left[\int_{\substack{closed\\CS}}(-p\mathbf{n}+\boldsymbol{\tau}_c)\cdot\mathbf{U}\,\mathrm{d}s + \int_{\substack{open\\CS}}(-p\mathbf{n}+\boldsymbol{\tau}_o)\cdot\mathbf{U}\,\mathrm{d}s\right]$$

$$-\frac{\partial}{\partial t}\int_{\substack{control\\vol}}[\rho U^2 + \rho_{structure}U^2_{structure}]\,\mathrm{d}v$$

$$+\int_{\substack{open\\CS}}\rho U^2(\mathbf{U}-\mathbf{V}_{control})\cdot\mathbf{n}\,\mathrm{d}s = 0. \tag{23}$$

We know that the integral over the control volume equals twice the total kinetic energies of the fluid and the structure $2T$, where $T = T_{fluid} + T_{structure}$. Now apply the control volume equation (13) to the quantity $\mathscr{L}_{system}$,

$$\mathscr{L}_{system} = \int_{system}(\hat{T}_{structure} + \hat{T}_{fluid} - \hat{\Pi}_{structure} - \hat{\Pi}_{fluid})\,\mathrm{d}v, \tag{24}$$

where the terms under the integral are intensive properties and have units of energy per unit volume, that is,

$$\int_{system}\hat{T}_i\,\mathrm{d}v = T_i, \quad \int_{system}\hat{\Pi}_i\,\mathrm{d}v = \Pi_i.$$

Then,

$$\frac{\mathrm{d}}{\mathrm{d}t}\mathscr{L}_{system} = \frac{\mathrm{d}}{\mathrm{d}t}\int_{system}(\hat{T}_{structure} + \hat{T}_{fluid} - \hat{\Pi}_{structure} - \hat{\Pi}_{fluid})\,\mathrm{d}v, \tag{25}$$

where

$$\frac{\mathrm{d}}{\mathrm{d}t}\int_{system}(\hat{T}_{structure} + \hat{T}_{fluid} - \hat{\Pi}_{structure} - \hat{\Pi}_{fluid})\,\mathrm{d}v$$

$$= \frac{\partial}{\partial t}\int_{\substack{control\\vol}}(\hat{T}_{structure} + \hat{T}_{fluid} - \hat{\Pi}_{structure} - \hat{\Pi}_{fluid})\,\mathrm{d}v$$

$$-\int_{\substack{open\\CS}}\frac{1}{2}\rho U^2(\mathbf{U}-\mathbf{V}_{control})\cdot\mathbf{n}\,\mathrm{d}s. \tag{26}$$

The integral over the *open control surface* accounts for the fluid entering the control volume (no incoming structure), and therefore *the term* $\frac{1}{2}\rho U^2$ represents *the fluid kinetic energy flux across the control surface*. There is also a possible change in potential energy of the fluid per unit mass e. If there is no cavitation, an approximation can be made that, on average, for every part of the fluid crossing the control surface with an increase in potential, there is an equivalent loss in potential in another region of the surface. Of course, if the flow as a whole gains or loses potential, this assumption is invalid. Thus, e is not included if the average flow is perpendicular to the gravitational vector.

Substitute this expression into equation (23) to find

$$\frac{\mathrm{d}}{\mathrm{d}t}\int_{\substack{control\\vol}}(\hat{T}_{structure}+\hat{T}_{fluid}-\hat{\Pi}_{structure}-\hat{\Pi}_{fluid})\,\mathrm{d}v-2\frac{\mathrm{d}}{\mathrm{dt}}(T_{fluid}+T_{structure})$$

$$+\int_{\substack{open\\CS}}\left[\rho U^2-\frac{1}{2}\rho U^2\right](\mathbf{U}-\mathbf{V}_{control})\cdot\mathbf{n}\,\mathrm{d}s$$

$$+\int_{\substack{closed\\CS}}(-p\mathbf{n}+\boldsymbol{\tau}_c)\cdot\mathbf{U}\,\mathrm{d}s+\int_{\substack{open\\CS}}(-p\mathbf{n}+\boldsymbol{\tau}_o)\cdot\mathbf{U}\,\mathrm{d}s=0,$$

and noting that $\mathrm{d}\Pi_{fluid}/\mathrm{d}t=0$, and simplifying,

$$\frac{\mathrm{d}(-T_{structure}-T_{fluid}-\Pi_{structure})}{\mathrm{d}t}+\int_{\substack{open\\CS}}\frac{1}{2}\rho U^2(\mathbf{U}-\mathbf{V}_{control})\cdot\mathbf{n}\,\mathrm{d}s$$

$$+\int_{\substack{closed\\CS}}(-p\mathbf{n}+\boldsymbol{\tau}_c)\cdot\mathbf{U}\,\mathrm{d}s+\int_{\substack{open\\CS}}(-p\mathbf{n}+\boldsymbol{\tau}_o)\cdot\mathbf{U}\,\mathrm{d}s=0. \tag{27}$$

Note that the factor $\mathrm{d}t$ in all terms have been eliminated. Also, each term in the equation represents a time rate of change of a work term. That is, $\dot{W}$ or $\dot{T}$, meaning that these are expression for *power*. Equation (27) can be put into the form of equation (19) as follows:

$$\frac{\mathrm{d}(T_{structure}-T_{fluid}-\Pi_{structure})^{\substack{control\\vol}}}{\mathrm{d}t}$$

$$=\int_{\substack{open\\CS}}\frac{\rho}{2}U^2(\mathbf{U}-\mathbf{V}_{control})\cdot\mathbf{n}\,\mathrm{d}s+\int_{\substack{closed\\CS}}(-p\mathbf{n}+\boldsymbol{\tau}_c)\cdot\mathbf{U}\,\mathrm{d}s$$

$$+\int_{\substack{open\\CS}}(-p\mathbf{n}+\boldsymbol{\tau}_o)\cdot\mathbf{U}\,\mathrm{d}s \tag{28}$$

The questions we address later are (1) the possible and optimal control volume configurations that are suitable for the problems at hand, and (2) whether we can select a control volume such that the open surfaces are prescribed, thus leading to a variational principle, rather than equation (28). First, however, we would explore equation (28) in more detail.

Equation (28) is a scalar equation, and therefore its evaluation and simplification will result in a single equation of motion for the oscillating structure where all the fluid energy results in a forcing function on the structure. Such an equation of motion is in the single-degree-of-freedom class of models for vortex-induced structural oscillations.

The structural terms on the left-hand side of equation (28),

$$\frac{\mathrm{d}(T_{structure}-\Pi_{structure})^{\substack{control\\vol}}}{\mathrm{d}t},$$

are found by expressing $T_{structure} + \Pi_{structure}$ in terms of structural displacements and velocities and then differentiating with respect to time. The remaining fluid term is related as follows:

$$\frac{\mathrm{d}(T_{fluid})_{vol}^{control}}{\mathrm{d}t} = \frac{\mathrm{d}}{\mathrm{d}t}\left(\frac{1}{2} m_{fluid} U^2\right)_{\substack{control \\ vol}} = (m_{fluid} U \dot{U})_{\substack{control \\ vol}}, \tag{29}$$

where m_{fluid} within the (open) control volume is constant. In the above, *control vol* respectively refers to either the closed one that hugs the structure, or the open one that is concentric with the closed one. Because of the matched boundary conditions at the interface, that is, fluid velocity equals structural velocity, the existence of this term includes the added mass effect that is included when a structure oscillates in a relatively dense medium. Since this term is evaluated experimentally and fed into the governing equation, any fluid dynamics that is a result of structural oscillation is implicitly included.

The terms on the right-hand side of equation (28) are the various components of the kinetic energy flux across the control surface. Equation (28) is, furthermore, a statement of the first law of thermodynamics where heat transfer and dissipation has been omitted.

In summary, the linking of Hamilton's principle for an unprescribed system with Reynolds transport theorem results in the first law of thermodynamics. A check of the dimensions of all expressions, including the rectilinear acceleration, shows that all the units are rate of work, or power, that is, for example, ft lb/s or W, depending on the chosen system of units.

Equation (28) can be written as

$$\begin{aligned} &\frac{\mathrm{d}(T_{structure} + \Pi_{structure})_{vol}^{control}}{\mathrm{d}t} + (m_{fluid} U \dot{U})_{vol}^{control} \\ &= \int_{\substack{open \\ CS}} \frac{\rho}{2} U^2 (\mathbf{U} - \mathbf{V}_{control}) \cdot \mathbf{n} \, \mathrm{d}s \\ &\quad + \int_{\substack{closed \\ CS}} (-p\mathbf{n} + \boldsymbol{\tau}_c) \cdot \mathbf{U} \, \mathrm{d}s + \int_{\substack{open \\ CS}} (-p\mathbf{n} + \boldsymbol{\tau}_o) \cdot \mathbf{U} \, \mathrm{d}s. \end{aligned} \tag{30}$$

We envision the following procedure for working with equation (30). We will substitute expressions for the kinetic energies on the left-hand side. On the right-hand side, we will have experimentally based analytical expressions for the flow velocities, pressures and stresses. This relation will allow the derivation of an expression for the acceleration of the structure. This will be integrated twice to find the expression for the structural displacement as a function of time and the system parameters. This result will then be compared to the experimentally derived structural displacement as a function of time. The two functions will be compared, permitting an evaluation of the analytical framework and its components.

4.1.1. *Control volume definition*

First let us describe the control volume of interest here. Consider a top view of a circular cylinder with two control surfaces, one at the surface of the cylinder and the other some concentric distance out in the surrounding water. One question that arises when considering various possible control volumes is whether a particular control volume has

significant advantages either for the analytical formulation or for the experimental procedures, the results of which are required as input to the analytical model. This will have to be considered as part of an examination of the proposed methodology.

4.2. COUPLED EXPERIMENTS

There is no possibility of analytically arriving at expressions for each term and each function in equation (30). Therefore, it is necessary that an experimental program is run in parallel for particular applications. The power of this energy-based approach is two-fold. One is that an analytical framework is created to organize our understanding of a complex non-linear and interactive phenomenon. The other which is equally important is that the experimental program provides us with invaluable information about some of the components of these equations, and this permits us to utilize the variational tools in the derivation of the equations of motion.

5. SIMPLE EXAMPLE PROBLEMS

Several example problem formulations are presented next. These are, of course, simple cases meant to initiate us to the application of the general equation. It is straightforward to add structural and other damping mechanisms.

5.1. ANNULAR CONTROL VOLUMES MOVING IN TANDEM

Specifically, in the case of a two-dimensional idealized oscillation of a rigid cylinder, there will be one generalized co-ordinate, say $x(t)$. Then, the kinetic energy of the structure is related to $\dot{x}^2$ and the strain energy in the supporting springs (with net stiffness constant equal to k) will be related to x^2. The speed of the closed and open control volumes are $\dot{x}$, since they are defined to move with the structure. Similarly, the relative rectilinear accelerations of the closed and open control volumes are $\ddot{x}$. The expressions required to evaluate the terms $(-p\mathbf{n}+\boldsymbol{\tau}_c)\cdot\mathbf{U}$, and $(-p\mathbf{n}+\boldsymbol{\tau}_o)\cdot\mathbf{U}$ are determined experimentally. It has been assumed that the cylinder oscillates in the plane perpendicular to the flow direction, and that the acceleration (of the closed control volume) is rectilinear.

For this rigidly translating cylinder, we have

$$\frac{\mathrm{d}(T_{structure}+\Pi_{structure})^{control}_{vol}}{\mathrm{d}t}=\frac{\mathrm{d}}{\mathrm{d}t}\left(\frac{1}{2}m_{cylinder}\dot{x}^2+\frac{1}{2}kx^2\right)=\dot{x}(m_{cylinder}\ddot{x}+kx).$$

Equation (30) for this particular example can be written as

$$\dot{x}(m_{cylinder}\ddot{x}+kx)+m_{fluid}U\dot{U}$$

$$=\int_{\substack{open\\CS}}\frac{1}{2}\rho U^2(\mathbf{U}-\dot{\mathbf{x}})\cdot\mathbf{n}\,\mathrm{d}s+\int_{\substack{closed\\CS}}(-p\mathbf{n}+\boldsymbol{\tau}_c)\cdot\mathbf{U}\,\mathrm{d}s+\int_{\substack{open\\CS}}(-p\mathbf{n}+\boldsymbol{\tau}_o)\cdot\mathbf{U}\,\mathrm{d}s,$$

where, in this simplified problem, $\mathbf{V}_{control}=\dot{\mathbf{x}}=\dot{x}$, the last equality is due to the fact that the structural and outer fluid control volumes are stipulated to travel only in the x direction

perpendicular to the flow. The *open* and *closed* control surfaces refer to the outer and inner control surfaces, respectively. The expression $m_{fluid}U\dot{U}$ refers to the fluid between the two concentric control surfaces. $\Pi_{structure}$ includes all the potential stored in the structure. Because the motion of the cylinder is pure translation perpendicular to the gravitational field, we do not see the net force resulting from the difference between cylinder weight and buoyancy force. This net force acts along the axis of the cylinder.

Combining like terms yields

$$\dot{x}(m_{cylinder}\ddot{x} + kx) + m_{fluid}U\dot{U} = \int_{\substack{closed\\CS}} (-p\mathbf{n} + \boldsymbol{\tau}_c)\cdot\mathbf{U}\,\mathrm{d}s + \int_{\substack{open\\CS}} \left[\frac{1}{2}\rho U^2(\mathbf{U} - \dot{\mathbf{x}})\cdot\mathbf{n} + (-p\mathbf{n} + \boldsymbol{\tau}_o)\cdot\mathbf{U}\right]\mathrm{d}s. \tag{31}$$

5.2. STATIONARY OUTER CONTROL VOLUME: TRANSLATING CYLINDER

If the open control surface is stationary, while the inner control surface attached to the cylinder is still in motion as before, then $\dot{x} = 0$ in the integral over the open control surface, and we have the simplified equation,

$$\dot{x}(m_{cylinder}\ddot{x} + kx) + m_{fluid}U\dot{U} = \int_{\substack{closed\\CS}} (-p\mathbf{n} + \boldsymbol{\tau}_c)\cdot\mathbf{U}\,\mathrm{d}s + \int_{\substack{open\\CS}} \left[\frac{\rho}{2}U^2\,\mathbf{U}\cdot\mathbf{n} + (-p\mathbf{n} + \boldsymbol{\tau}_o)\cdot\mathbf{U}\right]\mathrm{d}s. \tag{32}$$

It is important to note that even in a free vibration in an initially still fluid, the flow velocity $U \neq 0$ since any motion of the structure from non-zero initial conditions will result in a fluid motion. Therefore, the equation of motion does not reduce here to $m_{cylinder}\ddot{x} + kx = 0$ even though $U(0) = 0$.

5.3. STATIONARY OUTER CONTROL VOLUME: CYLINDER OSCILLATING ABOUT CONTACT AT BASE

Here we take the cylinder to be connected only at its base via a leaf spring. It behaves like a column supported only at its base. For purposes of this example we assume that the cylinder is rigid, as above, and that three-dimensional effects can be ignored. The single generalized co-ordinate that defines the cylinder location is the angle of rotation θ rad. We have an additional term in the potential of the structure due to the difference between the buoyancy force and the weight. We assume that the resultants of these distributed forces act at the center of geometry of the circular cylinder. Then, for some rotation θ, this additional potential results in the moment $(mg - B)(L/2)\sin\theta$, where mg is the weight of the cylinder, B is the total buoyancy force (which equals the weight of the displaced fluid) and L is the length of the cylinder. Let I_o be the mass moment of inertia for the circular cylinder about its base, k_T be the torsional spring constant at the base, then the governing equation is

$$\dot{\theta}\left(I_o\ddot{\theta} + k_T\theta - (mg - B)\frac{L}{2}\sin\theta\right) + m_{fluid}U\dot{U} = \int_{\substack{closed\\CS}} (-p\mathbf{n} + \boldsymbol{\tau}_c)\cdot\mathbf{U}\,\mathrm{d}s + \int_{\substack{open\\CS}} \left[\frac{\rho}{2}U^2\mathbf{U}\cdot\mathbf{n} + (-p\mathbf{n} + \boldsymbol{\tau}_o)\cdot\mathbf{U}\right]\mathrm{d}s. \tag{33}$$

This equation, as well as the other cases above, can also be evaluated numerically if written in the form

$$\frac{1}{2}\frac{\mathrm{d}}{\mathrm{d}t}\{I_o\dot{\theta}^2 + k_T\theta^2 + (mg - B)L\cos\theta\} = F(t), \tag{34}$$

where $F(t)$ is the sum of all the remaining terms,

$$F(t) = -m_{fluid}U\dot{U} + \int_{\substack{closed\\CS}} (-p\mathbf{n} + \boldsymbol{\tau}_c)\cdot\mathbf{U}\,\mathrm{d}s + \int_{\substack{open\\CS}} \left[\frac{\rho}{2}U^2\mathbf{U}\cdot\mathbf{n} + (-p\mathbf{n} + \boldsymbol{\tau}_o)\cdot\mathbf{U}\right]\mathrm{d}s.$$

Then, we solve for θ by integrating both sides of equation (34), and then integrating again with respect to time. There are numerical issues to be resolved due to the complexities of the functions on both sides of the equals sign. A model problem is presented subsequently. We first present a brief discussion on the experimental apparatus used and the kinds of data that are obtained.

6. BACKGROUND TO EXPERIMENTAL WORK

This section describes the experimental methodology used to acquire key modeling data, i.e., kinetic energy transport and work by viscous forces across the boundaries of an integral control volume. There is also a presentation of preliminary data and their application to a prototype model.

Observe that equation (28) is an integral energy transport equation. The left-hand side represents the time rate of change of mechanical energy in the control volume. This includes time derivatives of kinetic and potential energies of the structure, and temporal variations of the fluid kinetic energy. The rate of change of fluid kinetic energy for a fixed control volume location, as well as the apparent change in fluid kinetic energy due to motion of the control volume through a spatially varying flow field, is included.

The right-hand side contains integral terms describing transport of fluid energy across the boundaries of the control volume. These are the fluid "forcing" functions which "drive" the structural motion, written in terms of energy transport. Specifically, the first term represents the net flux of fluid kinetic energy across the boundaries of the control volume. The other integrals are a mathematical description of the work done on the control volume boundaries by pressure and viscous forces, that is, the non-conservative surface forces.

6.1. EXPERIMENTAL DATA AS ANALYTICAL MODELLING INPUT

Solutions to equation (28) will be time-dependent expressions for the structure's motion as functions of both time and position along the structure. Attaining scientifically rigorous solutions, in turn, requires spatially and temporally resolved descriptions of the fluid "forcing" functions on the right-hand side as well as the fluid kinetic energy derivative on the left. Unfortunately, there is, as yet, no known generalized analytic solution to the fluid equations which could be integrated to obtain the necessary forcing functions. This tends to be a universal problem faced by modellers once the governing equations of motion have been derived.

When considering how to proceed, one immediately recognizes the risk of making assumptions without a clear understanding of the flow–structure interactions over the entire range of conditions being modelled. No matter how physically reasonable, there is a significant risk of introducing empiricism into the final solution. Without additional guidance, we would also lack the insight and confidence to realistically assess the versatility of the model.

Recent advances in video-based flow measurement techniques have enabled accurate measurement of derivative flow quantities in highly complex, turbulent flows. In particular, Shah *et al.* [34, 35] have used highly resolved digital particle image velocimetry (DPIV) data to compute terms in the vorticity transport equation, along with turbulent strain rates in a turbulent tip-vortex shed from a half Δ-wing. Hsu *et al.* [36] presented turbulent kinetic energy transport quantities obtained from DPIV measurements in a turbulent boundary layer.

In this paper, we look to capitalize on the power of DPIV and apply it to the modelling problem outlined above. Specifically, we show how high-resolution DPIV can be used to measure fluid energy transport terms and use that information as input to a reduced-order analytical fluid–structure interaction model. We also use experiments as a validation of the model output because the structure's position is inherently part of the acquired experimental data.

It is critical to note at the outset that DPIV is 'only' a two-dimensional, velocity field measurement technique. While information about pressure variations and contributions from three dimensionalities in the flow are not yet accessible, we demonstrate in this paper the power of integrating focused experiments with the analytics into a new modelling paradigm. Discussions of current limitations and possible solutions are included at appropriate points.

7. THE MODEL PROBLEM

A key objective of the present work is to prove the concept of integrating detailed experiments with reduced-order analytical modelling. In this context, we chose a geometrically simple model problem in which the fluid–structure interactions were fully coupled. That is, flow excited structural motions that, in turn, modulate the flow. Mathematical or experimental complexities, such as strong three dimensionality, were deferred for future development.

The model problem addressed in this study was the vortex-induced motion of a low mass-ratio circular cylinder. The cylinder was restrained at its bottom end by a leaf spring with freedom to move in the cross-stream plane only. A schematic drawing of this model problem is shown in Figure 1. One can think of it as an inverted pendulum excited by its own periodic vortex shedding. As will be described in greater detail, the amplitude of motion of the free, upper end was sufficiently small that the flow could be considered to be normally two-dimensional.

The physical model used in this study was a 2·54 cm diameter (D) cylinder constructed of thin wall aluminium tube. It was 128 cm long and immersed in a uniform flow of water $\sim$ 107 cm deep. The mass ratio was 1·53, the damping ratio was 0·054, and the cylinder natural frequency, f_n, was 1·25 Hz. For a detailed description of the cylinder and preliminary observations of the associated flow dynamics, the reader is referred to Atsavapranee, *et al.* [37].

The frequency and amplitude response characteristics of the cylinder are shown in Figure 2. Measurements were made at the cylinder mid-height, $\sim$ 70 cm above the floor of the water

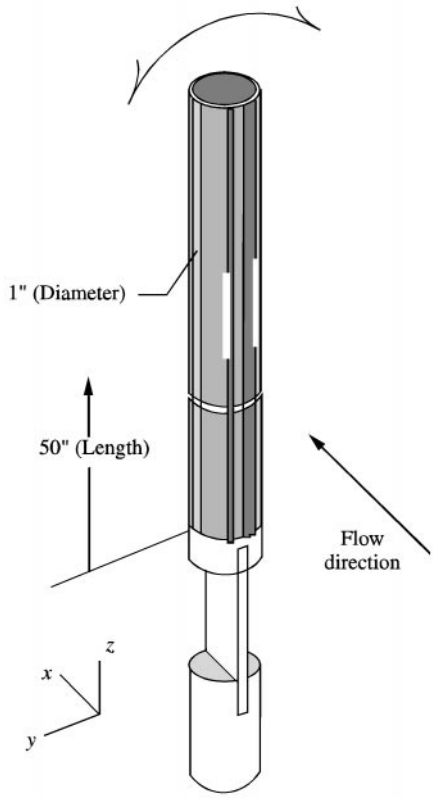

Figure 1. Schematic drawing of the oscillating cylinder experiment. Observe that the bottom end was fixed to the water tunnel floor by a leaf spring while the top end was free to move.

tunnel. Open circles and squares indicate cylinder amplitude for different non-dimensional flow speeds. The x's denote frequencies of both vortex shedding and cylinder oscillation. At speeds where frequencies are indicated by x's, the two frequencies were identical. At the low and high ends of the speed range covered in Figure 2, there was no appreciable cylinder motion. For these cases, Karman vortex shedding frequencies are indicated by open diamonds. Also included in the plot is a solid line denoting a Strouhal number of 0·21, the non-dimensional Karman shedding frequency for a stationary cylinder. There is also a shorter dashed line indicating a Strouhal number of 0·18.

A salient feature of Figure 2 is the existence of three distinct regimes in the frequency–amplitude response curves. For a detailed discription and analysis of these regimes, see Atsavapranee *et al.* [37]. At the low-speed end, $3 = U/f_n D = 4$, there was a low-amplitude oscillation of the cylinder with a characteristic beating behavior. This was referred to as the "pre-synchronization" regime. Regime II, between non-dimensional speeds of 4 and 5·5, was named the "resonant synchronization" regime because the vortex shedding and cylinder motion were so well co-ordinated that the amplitude of motion was a maximum. The vortex shedding and cylinder oscillation frequencies appeared to have a Strouhal number of 0·18, as shown in Figure 2. Though significantly diminished, the beating phenomenon observed in Regime I was still present in Regime II. Sample time traces of cylinder amplitude at the mid-height of the cylinder for each of the three regimes being identified are shown in Figure 3.

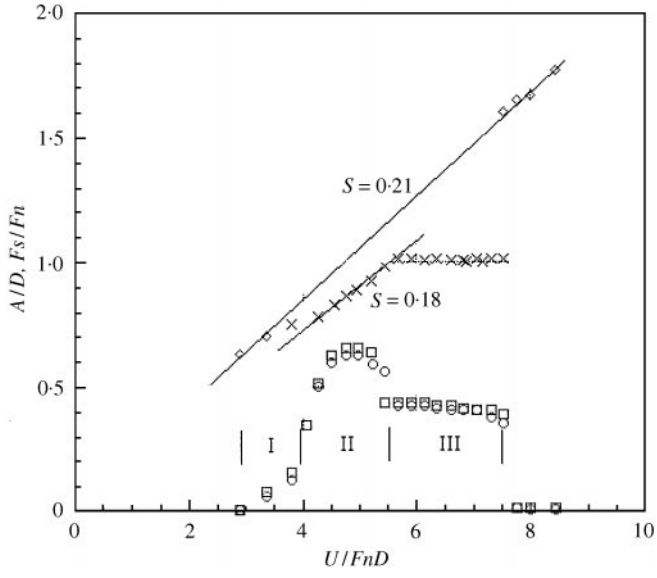

Figure 2. Frequency amplitude response plot for the inverted pendulum experiment shown in Figure 1. □, ○, Cylinder amplitude for two independent but identical experimental runs; ×, cylinder oscillation and vortex shedding frequency for conditions in which vortex induced vibration occurs; ◇, vortex shedding frequency for conditions where the cylinder remains stationary. Regions identified as I, II and III denote the 'pre-synchronization', 'resonant synchronization', and 'classic lock-in' regimes.

The final regime, $5{\cdot}5 = U/f_nD = 7{\cdot}5$, was the 'classic lock-in' regime. In this regime, the cylinder oscillation frequency and amplitude remained constant over a wide range of flow speeds. Flow visualization studies reported in the aforementioned reference indicated that in the classic lock-in regime, the flow was modulated by the cylinder motion. That is, the vortex shedding appeared rather disorganized in comparison to the pre- and resonant synchronization regimes. We interpret this to mean that the cylinder modulated the flow so that 'just enough' energy was transferred from fluid to structure to maintain a fixed amplitude oscillation at the natural frequency.

With this brief overview, we now turn to the experimental methodology issues necessary to bring about a reduced order analytical solution for this problem. We begin in the next section with a description of the experimental facilities and techniques. This is followed by a presentation of DPIV measurements analyzed and presented in a form that is accessible to the modelers. Then, we present preliminary model results and a discussion of issues yet to be addressed.

7.1. EXPERIMENTAL APPARATUS AND METHODS

7.1.1. *Flow facility*

Experiments were conducted in the free surface water tunnel facility at Rutgers University. Top and side view schematic diagrams of the facility appear in Figure 4. The closed-circuit tunnel consisted of an upstream settling chamber, two-dimensional contraction, test section, downstream end tank, pumps, and piping. Note that the pumps are not shown in Figure 4. Details of the flow facility may be found in Smith [38] and Grega *et al.* [39].

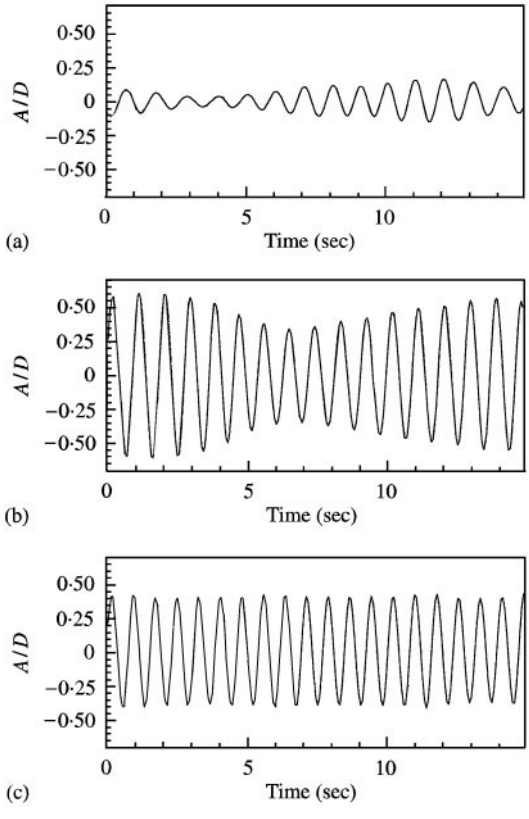

Figure 3. Plots of cylinder position versus time for the three different oscillation regimes identified in Figure 2: (a) 'pre-synchronization', $U/f_nD = 3{\cdot}8$; (b) 'resonant synchronization', $U/f_nD = 4{\cdot}8$, and the (c) 'classic lock-in', $U/f_nD = 6{\cdot}1$.

The test section measured 58·4 cm in width × 122 cm in depth × 610 cm in length. It was constructed entirely from 1·91 cm thick glass panels placed in a welded steel I-beam frame. Flow was driven by two pumps operating in parallel. Variable speed controllers were used to set the flow rate between 760 and 15,000 l/min. With the test section completely filled, the maximum flow rate corresponded to a mean free stream velocity of approximately 30 cm/s. Free stream turbulence levels were less than 0·1% of the mean free-stream velocity and the flow was uniform across the cross-section to within 2%.

7.1.2. *Video Imaging and Capture*

Video images for the DPIV studies were made using a Kodak Megaplus ES1·0 video camera with 1024 × 1024 pixel resolution at a framing rate of 30 frames per second. Pairs of consecutive video frames comprising DPIV video image pairs were captured and stored in a Pentium computer. The flow was illuminated using the beam from a Coherent Innova 70-5 5 W argon ion laser which was swept into sheets of light using a galvanometer driven by a custom laser sweep circuit described briefly in the following paragraph. A drawing of the optics set-up is shown in Figure 5.

The primary function of the laser sweep/timing circuit was to generate an input signal to pivot a small front surface mirror mounted on the shaft of a small galvanometer; when the

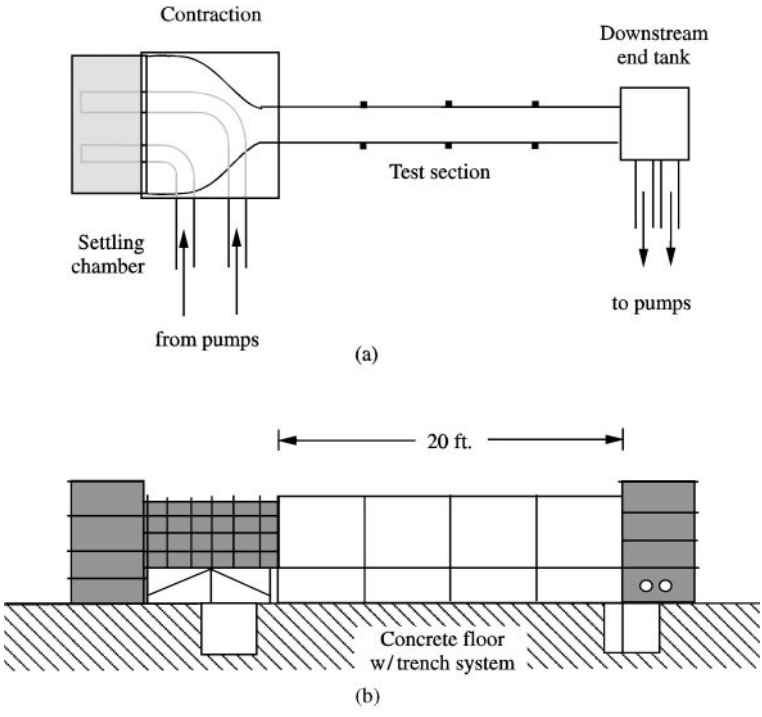

Figure 4. (a) Top and (b) side view sketch of the Rutgers free surface water tunnel.

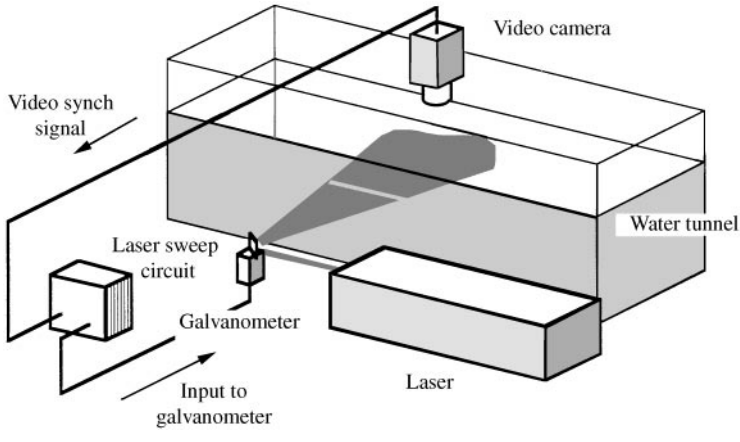

Figure 5. Oblique view drawing of the laser diagnostic system installed in the Rutgers free surface water tunnel. Note that the video signal is sent to the Laser Sweep Circuit to synchronize the Galvanometer motion.

shaft rotated, a laser beam reflecting off the mirror swept out a sheet of light. The galvanometer input signal consisted of pairs of closely spaced voltage ramps that caused the galvanometer shaft to rotate at a constant rotation speed to produce pairs of closely timed, short duration, laser sheets. Use of the sweep circuit made it possible to reduce the effective time between frames, Δt, to a few milliseconds by producing one sheet at the end of one video frame and a second sheet shortly thereafter at the beginning of the next frame. One

limitation of this technique, of course, is that one can only obtain image pairs at a rate of 15 Hz. A modification of the DPIV technique, which we named digital particle image accelerometry (DPIA), will permit accurate measurement of fluid acceleration even at this relatively low-data acquisition rate. This is briefly described later in this paper. A complete documentation of the technique may be found in Dong *et al.* [40].

7.1.3. *DPIV Processing Program*

The high-resolution DPIV software package employed in Shah *et al.* [34, 35] was also used for this investigation; a detailed description of this program, its calibration, and accuracy is provided in Hsu [41]. The essence of the program is identical to that developed by Willert and Gharib [42]. That is, cross-correlations of user-specified interrogation windows are computed in Fourier transform space to determine the mean displacement of particles contained in the windows. The principle feature of the current program is the two-step correlation process. First, a 'coarse' particle displacement field is generated using large, overlapping 128 pixel $\times$ 128 pixel interrogation windows. The resulting displacement field is very accurate, i.e., free of obviously errant vectors, but also highly spatially averaged.

The coarse displacement field is then used as a particle displacement estimator for a "fine" correlation stage. For these experiments, fine interrogation windows were 64 pixels $\times$ 64 pixels with 16 pixels between vectors. A key feature of the fine correlation stage is the offset between interrogation windows in each frame comprising a DPIV image pair. The interrogation window in Frame 2 was offset relative to its counterpart in Frame 1 by an amount determined from local interpolation of the coarse displacement field. In this manner, it was possible to accurately compute particle displacements larger than the fine interrogation window dimensions. Again the fine windows are incremented using quarter window sized steps.

The end result is a processing program capable of generating extremely clean DPIV vector fields. A sample velocity vector field taken in the wake of a freely oscillating cylinder appears in Figure 6. In this example, the Reynolds number of the flow was 3800, corresponding to the resonant synchronization regime shown in Figure 2. A reference velocity equal to half the free stream was subtracted from every vector to help visualize the vortices. Note the absence of any obviously 'bad' vectors, and the overall smoothness of the streamlines. Uncertainty analysis for velocity and their derivative quantities for measurements of this type are presented in Shah *et al.* [34] and Hsu *et al.* [36]. As will be seen in the following section, the resolution and accuracy of the measurements enabled accurate assessment of terms 2 and 3 in the energy equation (33).

7.1.4. *Experimental Results*

As reported in Atsavapranee *et al.* [37], DPIV measurements were made over a wide range of Reynolds numbers spanning the resonant synchronization, II, and classic lock-in, III, regimes. In this paper, our intent was to examine the process of incorporating a single data set into a reduced-order analytical model. We chose therefore to focus on a single case in Regime II because of the high degree of synchronization between vortex shedding and cylinder motion. The specific case we chose was flow at a Reynolds number of 3800, or a non-dimensional velocity, $U/f_n D = 4{\cdot}8$. This corresponded to the peak in the amplitude response plot shown in Figure 2 and the time trace shown in Figure 3(b). The data set for this case consisted of 225 consecutive DPIV velocity field measurements taken at 66 ms intervals, or $\sim 1/14$ of a cylinder oscillation period, in a horizontal plane perpendicular to the axis of symmetry of the cylinder at rest. The location of the measurement plane was ~ 70 cm above the floor of the test section coinciding with the amplitude measurements.

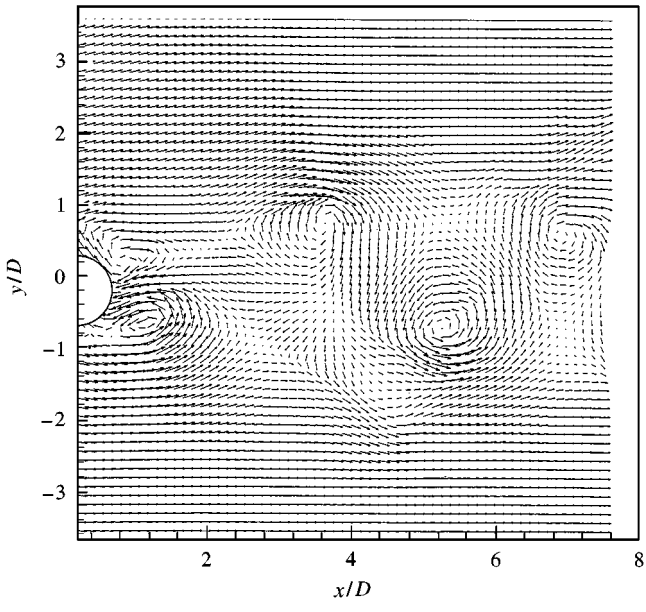

Figure 6. Sample instantaneous vector plot showing the wake of the cylinder in the resonant synchronization regime. The streamwise velocity components have been reduced by 7·5 cm, half the free stream speed, to better visualize the Kármán vortices in the wake. Flow is left-to-right with the cylinder appearing on the left side of the plot.

The spacing between vectors was 0·12 cm corresponding to $\lambda/D = 0{\cdot}05$. The total duration of the sample was 15 s, or 16 cylinder oscillation periods. In this section, we present detailed data for this case.

The first step in providing experimental support for the modelling effort was to compute key contributions in equation (28) that are accessible from each of the 225 instantaneous vector fields. Figures 7 and 8 each show sample time sequences containing six instantaneous contour plots of energy transport terms over one oscillation period. Flow in these plots is from left-to-right; the down-stream half of the cylinder is indicated by a half circle along the left edge of the plots. Contour values in all plots are dimensional with units of g cm^2/s^3. For reference, corresponding velocity vectors were superimposed on the contour plots. Again, a reference velocity of $U_\infty/2$ has been subtracted to highlight the individual Karman vortices.

Figure 7 contains contours of instantaneous local kinetic energy flux in the streamwise direction, values of the integrand $\rho(u^2 + v^2)u/2\,\mathrm{d}y$, computed at each vector location. Note that lower-case velocity components, u and v, denote instantaneous local values. The corresponding flux of kinetic energy in the cross-stream direction was also calculated but is not shown.

Figure 8 shows the rate of viscous work done in the cross-stream direction acting on streamwise, dx elements, $(\tau_{xy}u + \tau_{yy}v)\mathrm{d}x$. Contributions due to viscous forces acting on cross-stream, dy, elements are not shown. Derivatives were computed from the velocity vector fields using central differences except along the edges of the vector fields where one-sided differences were used. Observe that in comparison to the contour levels in Figure 7, the rate of work done by viscous forces is three orders of magnitude smaller than the kinetic energy flux.

We re-emphasize at this point the fact that we compute only those parts of the integral quantities which can be obtained from two-dimensional vector fields. Work is currently in

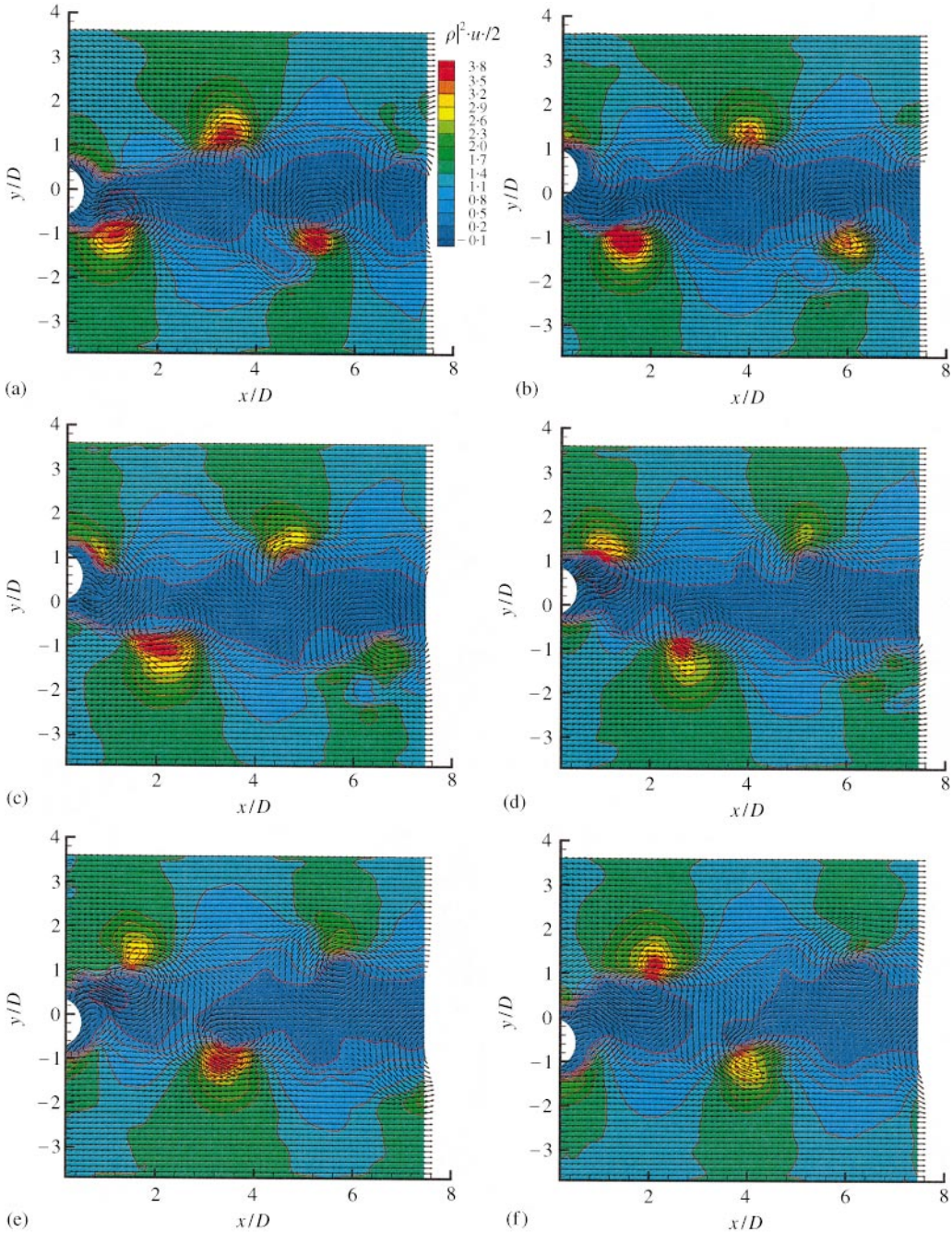

Figure 7. Series of six contour plots showing the flux of fluid kinetic energy across a vertical control volume element, one vector spacing in height. Flow is left-to-right with the instantaneous cylinder position indicated. The time between plots is 2/15 s. The corresponding velocity field is shown for reference.

progress to assess the validity of the quasi-two-dimensional assumption for the inverted pendulum problem. The findings of this study will be presented at a later date. As will be further discussed, we continue to work on obtaining temporally resolved acceleration

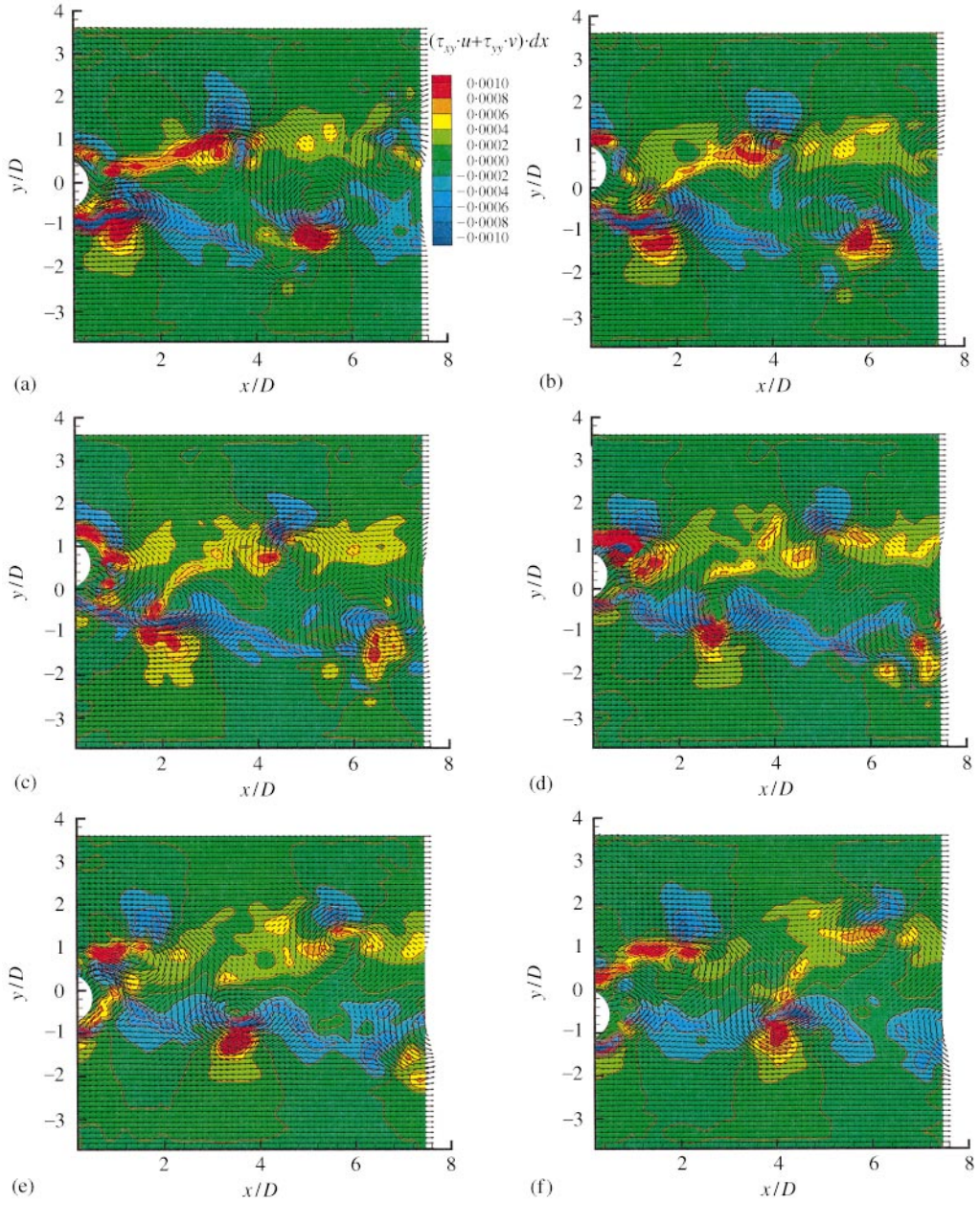

Figure 8. Series of six contour plots showing the rate of viscous work being done on a horizontal control volume element, one vector spacing in width. Flow is left-to-right with the instantaneous cylinder position indicated. The time between plots is 2/15 s. The corresponding velocity field is shown for reference.

information necessary for evaluating temporal derivatives of fluid kinetic energy. Specifically, resolution and accuracy issues associated with the DPIA technique described in Dong *et al.* [40] are being addressed and will be applied to this problem as well. Finally, determination of the rate of work due to pressure forces is also problematic at this time. In principle, this can be resolved using the approach described in Unal *et al.* [43]. Briefly

stated, if spatial and temporal velocity derivatives can be accurately determined in a quasi-two-dimensional flow, then one can back out the pressure field by integrating the differential Navier–Stokes equations.

Computing integrals for a desired control volume, then, simply required summing values along a predetermined control volume boundary. The control volume used for this exercise spanned 40 vectors in the cross-stream direction and 20 vectors in the streamwise direction. This was 1·85 and 0·92 cylinder diameters in the y and x directions respectively. The control volume was aligned with the left edge of the vector fields and centered in the cross-stream direction about the line of symmetry, $y/D = 0$. Note that, although this choice of control volume was necessary for the current data set, it is probably less than optimal because the entire upstream half of the cylinder is not included. For the purposes of demonstrating the data acquisition and analysis process, this is sufficient. However, it will be seen that the amplitude response predicted by the reduced-order model is approximately half of the measured cylinder amplitude. This is quite probably due to the fact that the integrated values of fluid kinetic energy flux contain only the downstream half of the structure. Measurements in which the cylinder is located in the center of the camera field of view are currently in progress to correct this problem.

Time histories of fluid energy transport terms obtained from the complete 225 field data sets are shown in Figure 9. Note that transport quantities have been non-dimensionalized by $\frac{1}{2}\rho U_\infty^3 L$, where L is the length of the upstream (or downstream) face of the control volume. This non-dimensionalization may be physically interpreted as

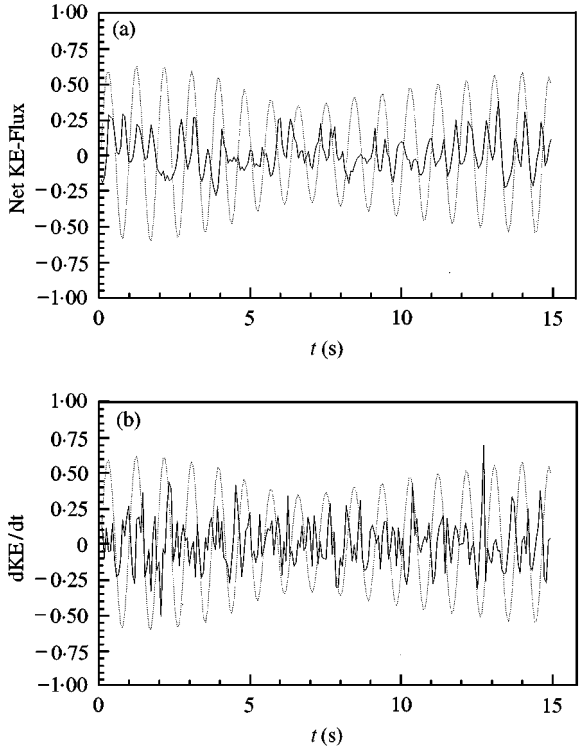

Figure 9. Time traces of (a) net fluid kinetic energy flux across the boundaries of a control volume, and (b) time rate of change of fluid kinetic energy within a control volume for the resonant synchronization case. Plots are non-dimensionalized by $1/2\rho U_\infty^3 L$. The corresponding cylinder position (non-dimensionalized by diameter) vs. time trace appears as a dotted line in both plots.

the total kinetic energy flux of the free-stream flow into a control volume with upstream dimension, L.

Figure 9(a) is a 15 s trace of net kinetic energy flux across the boundaries of a control volume. This appears as a solid line in the figure. Superimposed on the kinetic energy flux trace is a reproduction of the cylinder position, non-dimensionalized by cylinder diameter vs. time trace shown in Figure 3(b) with a dotted line. The position vs. time signal was obtained by locating the cylinder position in each of the captured video images. In this way, we know the exact cylinder position, velocity, and acceleration the moment the fluid transport terms were acquired.

A useful thing to keep in mind when examining this trace is that, for the resonant synchronization regime, a strong Karman vortex was being shed at about the same time the cylinder reached its maximum deflection. The implication of this to energy transport is readily apparent in the kinetic energy flux. There are two features of Figure 9(b) which warrant some conjecture. The first is the apparent correlation between peaks in the energy flux with peaks in cylinder motion. For the cylinder oscillation period of $\sim 0{\cdot}94$ s, observe the presence of a peak in the kinetic energy flux trace every $\sim 0{\cdot}47$ s. The coincidence of peaks in kinetic energy flux with maximum cylinder deflections is consistent with the visual observation of strong vortices being shed near maximum cylinder deflection. Note that the correlation appears strongest when the cylinder amplitudes are largest. In the range, $4 < t < 11$ s, where the oscillation amplitudes are reduced, the periodicity of the peaks in the kinetic energy flux is less apparent.

The second feature is the existence of longer time variations in Figure 9(a) that seems to correlate to the period of the beating phenomenon. In particular, if one takes a local running average of kinetic energy flux, say over a period of one cylinder oscillation cycle, it appears that there is a net kinetic energy flux out of the control volume when the peak-to-peak oscillation amplitudes are largest. Conversely, this running average becomes negative between 4 and 11 s when the peak-to-peak amplitude is smallest.

We recall at this juncture that kinetic energy fluxes out of the control volume are positive (because the area vector and velocity vector both point outward from the control surface). We then postulate that the long time variation observed in Figure 9(a) is fluid energy transport to/from the cylinder as a function of the peak-to-peak cylinder amplitude. When the amplitude is smallest, the cylinder draws energy from the flow to amplify the oscillations. During this time, the net kinetic energy flux is negative. When the cylinder reaches its maximum peak-to-peak amplitudes, it returns energy back to the fluid. This is observable as a positive, outward kinetic energy flux and as a tendency for the cylinder amplitude to begin decreasing again. One of the prime advantages of the current modelling approach is that we will be able to directly evaluate this hypothesis; such findings will be the topic of a subsequent paper addressing the dynamics of the fluid–structure interactions.

Figure 9(b) is a plot of variations in the rate-of-change of fluid kinetic energy within the control volume. These are estimates of the actual time derivatives computed using simple one-sided differences between successive velocity fields. Since the time between velocity fields was 1/15 s, it is likely that we have not resolved the peak accelerations. Again, the DPIA technique described in Dong *et al.* [39] will be employed in the subsequent detailed investigations of various oscillation regimes. For the purposes of demonstrating the application of experimental data of this type to an analytical modelling effort, the trace in Figure 9(b) will suffice.

Finally, we note that the rate of work done by viscous forces, both shear and elongational, on the control surface is negligibly small in comparison to the flux and time derivative terms shown in Figure 9. This is consistent with the contour plots shown in

Figures 7 and 8. For a reduced-order model, we will probably be able to neglect the contribution of non-conservative viscous forces for this class of problems.

8. APPLYING EXPERIMENTS TO THE REDUCED-ORDER ANALYTICAL MODEL

In the preceding section, we presented detailed flow measurements from an inverted oscillating pendulum experiment. The culmination of the analysis was a set of time traces of three key fluid kinetic energy transport terms, net kinetic energy flux, time rate of change of fluid kinetic energy, and rate of work done by viscous forces. The plots shown in Figure 9 are precisely the fluid "forcing" functions needed to analytically determine the motion of the cylinder. In this section, we show how these data were applied to the governing equation and compare the theoretical prediction of cylinder motion with the actual, experimentally measured oscillations.

The precise form of the equation of motion used in this analysis is equation (33). The equation was simulated using MATLAB in which the fluid forcing terms, appearing on the right hand side, were the experimentally determined functions presented in Figure 9. Since the experimental data were necessarily provided in the form of a discrete dataset with sampling points every 15th of a second, a fast Fourier transform was performed on the data within MATLAB. For this initial calculation, 100 terms in the Fourier-transformed signals were retained. Subsequent detailed analysis will be conducted to determine the minimum number of terms necessary to accurately model the cylinder dynamics.

A comparison between the actual cylinder motion and the motion predicted by our reduced-order model is shown in Figure 10. Figure 10(a) is again a reproduction of the cylinder position versus time trace for the resonant synchronization case shown in Figure 3(b). Figure 10(b) is the corresponding position versus time plot generated by the MATLAB

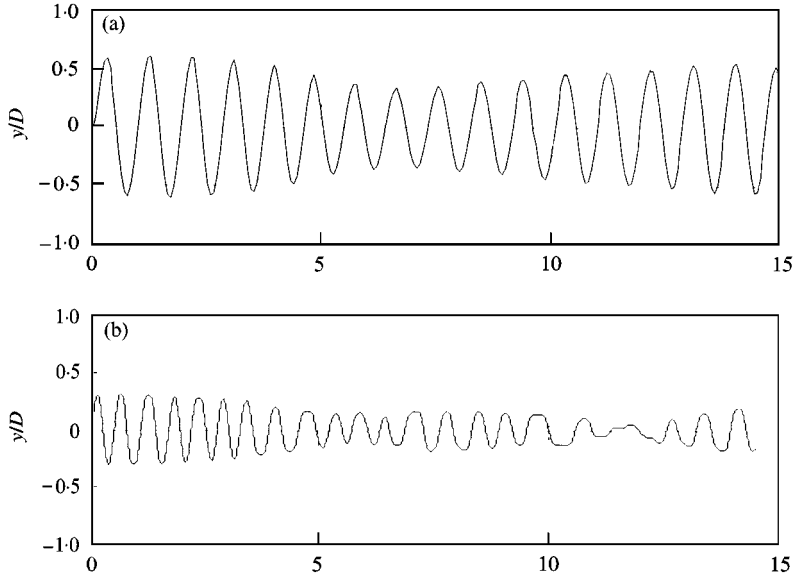

Figure 10. Comparison of (a) the actual cylinder position vs. time trace with the (b) computed results from the reduced-order model. Observe that the frequency and beating characteristics all appear to be captured by the model. Deviations in amplitude response may be due to the choice of experimental control volume. Abscissas of both plots are in seconds.

program. Observe that the oscillation frequency appears to be accurately predicted by the model along with the beating behavior. The predicted amplitude is approximately half of the measured amplitude. As noted in the preceding section, this is probably due to the fact that the experimental control volume included only the downstream half of the cylinder. We also note that there are several waveforms in the modelled response where the peaks appear as flattened plateaux. These can be seen at $t = 3, 7, 9$, and 11 s. We believe that these are the results of numerical instabilities in the MATLAB program; there is a singularity in the governing equation at the extremes of the cylinder motion where the structure velocity is zero. This is particularly problematic when the experimental data were acquired very close to the cylinder peak positions. At this juncture, we believe that the numerics are not sufficiently robust to smoothly integrate across these singularities, thereby resulting in artificially elongated peaks. Again, work is in progress to rectify this problem.

Nonetheless, the potential of the model to accurately predict the response of the cylinder to vortex-induced vibrations is extremely encouraging in the light of the refinement work yet to be done. Specific refinements being implemented include use of the new DPIA measurement capability. We are developing a trigger circuit which will enable phase-averaged measurements of the beating phenomena. Finally, we are adjusting the imaging field of view so that the cylinder appears in the center of the image. We are confident that these modifications will provide even more accurate, more highly resolved data sets which will facilitate a detailed understanding of the dynamic coupling of fluid–structure interactions.

9. A MORE GENERAL VARIATIONAL APPROACH

9.1. CONFIGURATION PRESCRIBED AT t_1 AND t_2

Suppose we prescribe the system at t_1 and t_2, then a variational formulation becomes possible. Begin with equation (17), repeated here,

$$\delta \int_{t_1}^{t_2} \mathscr{L}_{system}\, \mathrm{d}t + \int_{t_1}^{t_2} \mathrm{d}t \int_{\substack{open\\CS}} [(\boldsymbol{\sigma}\cdot\mathbf{n})\cdot\delta\mathbf{r} - \rho(\mathbf{U}-\mathbf{V}_{control})\cdot\delta\mathbf{r}(\mathbf{U}\cdot\mathbf{n})]\, \mathrm{d}s$$

$$+ \int_{t_1}^{t_2} \mathrm{d}t \int_{\substack{closed\\CS}} (\boldsymbol{\sigma}\cdot\mathbf{n})\cdot\delta\mathbf{r}\, \mathrm{d}s = 0,$$

and substitute equations (21) and (22) to find

$$\delta \int_{t_1}^{t_2} \mathscr{L}_{system}\, \mathrm{d}t + \int_{t_1}^{t_2} \mathrm{d}t \int_{\substack{open\\CS}} [(-p\mathbf{n}+\boldsymbol{\tau}_o)\cdot\delta\mathbf{r} - \rho(\mathbf{U}-\mathbf{V}_{control})\cdot\delta\mathbf{r}(\mathbf{U}\cdot\mathbf{n})]\, \mathrm{d}s$$

$$+ \int_{t_1}^{t_2} \mathrm{d}t \int_{\substack{closed\\CS}} (-p\mathbf{n}+\boldsymbol{\tau}_c)\cdot\delta\mathbf{r}\, \mathrm{d}s = 0. \tag{35}$$

The next step here would be to work with each term in order to arrive at an equation of the form

$$\int_{t_1}^{t_2} \left\{ \int_{\substack{physical\\domain}} [EOM]\delta\mathbf{r} + |[\cdots]\delta\mathbf{r}|_{boundaries} \right\} \mathrm{d}t = 0, \tag{36}$$

from which, using the argument that $\delta\mathbf{r}$ is arbitrary everywhere except at the boundaries at t_1 and t_2 leads to the equations of motion, *EOM*. There will be as many equations of motion as there are generalized co-ordinates in the system. The conditions $|[\cdots]\delta\mathbf{r}|_{boundaries} = 0$ lead to the possible boundary conditions. $\delta\mathbf{r}$ is a vector with dimension equal to the number of generalized co-ordinates. Our results using this approach can then be compared with that of the last section. At this time it is not possible to draw any specific conclusions, but we would like to expand a bit on this development, the details of which will appear in a subsequent paper.

We know that the Lagrangian of the continuous system, structure and fluid, is obtainable by standard methods, resulting in one equation of motion in each generalized co-ordinate. Assume, for a rectangular cross-section in the open control volume, that the ordinate is the co-ordinate y and the abscissa is the co-ordinate x, then the variation $\delta\mathbf{r}$ will be $\pm\,\delta y$ or $\pm\,\delta x$ respectively. Performing the variation of the Lagrangian also results in the respective boundary conditions. Formally, we have

$$\delta \int_{t_1}^{t_2} \mathscr{L}_{system}\,\mathrm{d}t = \int_{t_1}^{t_2} [(S_x + F_x)\delta x + (S_y + F_y)\delta y]\,\mathrm{d}t + BCs. \tag{37}$$

There then remains the need to expand the variations within the open and closed control volumes. Consider first the open control volume. We will find

$$\int_{t_1}^{t_2} \mathrm{d}t \int_{\substack{open\\CS}} [(-p\mathbf{n} + \boldsymbol{\tau}_o)\cdot\delta\mathbf{r} - \rho(\mathbf{U} - \mathbf{V}_{control})\cdot\delta\mathbf{r}(\mathbf{U}\cdot\mathbf{n})]\,\mathrm{d}s$$

$$= \int_{t_1}^{t_2} \mathrm{d}t\ \{[(O_x)\delta x + (O_y)\delta y]\}. \tag{38}$$

For the inner control volume, the cross-section is circular. Therefore, the outward normal $\delta\mathbf{r}$ will be of the form $\delta\mathbf{r} = \pm\cos\delta\mathbf{x} \pm \sin\delta\mathbf{y}$. Then,

$$\int_{t_1}^{t_2} \mathrm{d}t \int_{\substack{closed\\CS}} (-p\mathbf{n} + \boldsymbol{\tau}_c)\cdot\delta\mathbf{r}\,\mathrm{d}s = \int_{t_1}^{t_2} \mathrm{d}t\{[(C_x)\delta x + (C_y)\delta y]\}. \tag{39}$$

Equation (35) then becomes

$$\int_{t_1}^{t_2} [(S_x + F_x + O_x + C_x)\delta x + (S_y + F_y + O_y + C_y)\delta y]\,\mathrm{d}t + BCs = 0. \tag{40}$$

Functions S, F, O, and C are those that arise from the surface integration. *BCs* are the boundary conditions. Using the familiar arguments that since the variations are arbitrary and independent, the only way that the integral can be identically zero is if each factor of the variations equals zero, we have

$$S_x + F_x + O_x + C_x = 0, \quad S_y + F_y + O_y + C_y = 0. \tag{41, 42}$$

These two equations are the two, non-linear coupled partial differential equations that are the reduced-order model for the fluid–structure interaction. It is important to emphasize

that we chose two generalized co-ordinates in order to demonstrate the procedure. There will be as many coupled partial differential equations as there are generalized co-ordinates. For example, if the structural model can bend in two co-ordinates as well as extend, then it alone will have three generalized co-ordinates. We expect to be able to model more realistic fluid–structure interaction problems. This work is progressing.

10. DISCUSSION AND CONCLUSIONS

The work of McIver has been extended to model the oscillation of a structure in a fluid flow. Two variational approaches have been developed. The first approach assumes that the system configuration is *not* prescribed at the end times. This led to a single equation governing the motion of the structure as it is coupled to the fluid system. This equation has the units of power, and is therefore a power balance between fluid and structure. The second approach which is only introduced and will be fleshed out in a subsequent paper follows the more traditional variational approach of prescribing the system configuration at the end times. As outlined, this approach will result in a series of governing equations, one for each degree of freedom. This approach holds promise for more complicated flow patterns and structural behavior.

The above theoretical developments rest heavily in a practical and literal sense upon experimental input. The derived governing equations are semi-empirical, requiring experimentally developed functions. However, this is certainly an explicit trademark of all fluid mechanics, and is implicit in all of science and engineering. We view it as a positive aspect of the model, that it is inexorably linked to physical data. The second part of this paper developed the details of the concurrent experimental program.

ACKNOWLEDGMENTS

This work was supported by the Office of Naval Research Grant No. N00014-97-1-0017. We would like to thank our program manager Dr. Thomas Swean for his interest and financial support. We also acknowledge the computational support of Mr. Steven Kuchnicki in developing and running the MATLAB code for this paper and Ms. Peng Dong for assistance with the experimental program.

REFERENCES

1. R. T. HARTLEN and I. G. CURRIE 1979 *Journal of the Engineering Mechanics Division, Proceedings of the American Society of Civil Engineers*, 577–591. Lift-oscillator model of vortex-induced vibration.
2. A. W. MARRIS 1964 *Journal of Basic Engineering*, 185–196. A review on vortex streets, periodic wakes, and induced vibration phenomena.
3. E. BERGER and R. WILLE 1972 *Annual Review of Fluid Mechanics* **4**, 313–340. Periodic flow phenomena.
4. R. KING 1977 *Ocean Engineering* **4**, 141–171. A review of vortex shedding research and its applications.
5. T. SARPKAYA 1979 *Journal of Applied Mechanics* **46**, 241–258. Vortex-induced oscillations: a selective review.
6. K. Y. R. BILLAH 1989 *Ph.D Dissertation, Department of Civil Engineering and Operations Research, Princeton University*, A study of vortex-induced vibration.
7. M. M. ZDRAVKOVICH 1996 *Journal of Fluids and Structures* **10**, 427–437. Different modes of vortex shedding: an overview.

8. S. BALASUBMRAMANIAN and R. A. SKOP 1999 *Proceedings of the 13th ASCE Engineering Mechanics Division Specialty Conference*, *Johns Hopkins University*, *Baltimore*, 13–16 *June* (CD-ROM). Vortex-excited dynamics of a tapered pivoted cylinder in uniform and shear flows.
9. H. BARHOUSH, A. H. NAMINI and R. A. SKOP 1995 *Journal of Sound and Vibration* **184**, 111–127. Vortex shedding analysis by finite elements.
10. Y. CAI and S. S. CHEN 1996 *Journal of Sound and Vibration* **196**, 337–349. Dynamic response of a stack/cable system subjected to vortex induced vibration.
11. S. S. CHEN, S. ZHU and Y. CAI 1995 *Journal of Sound and Vibration* **184**, 73–92. An unsteady flow theory for vortex-induced vibration.
12. C. F. CHRISTENSEN and J. B. ROBERTS 1998 *Journal of Sound and Vibration* **211**, 617–636. Parametric identification of vortex-induced vibration of a circular cylinder from measured data.
13. L. GOSWAMI, R. H. SCANLAN and N. P. JONES 1993 *Journal of Engineering Mechanics* **119**, 2270–2302. Vortex-induced vibration of circular cylinders I: experimental data.
14. H. GUPTA, P. P. SARKAR and K. C. MEHTA 1996 *Journal of Engineering Mechanics* **122**, 1031–1037. Identification of vortex-induced-response parameters in time domain.
15. F. S. HOVER, S. N. MILLER and M. S. TRIANTAFYLLOU 1997 *Journal of Fluids and Structures* **11**, 307–326. Vortex-induced vibration of marine cables: experiments using force feedback.
16. I. JADIC, R. M. C. SO and M. P. MIGNOLET 1998 *Journal of Fluids and Structures* **12**, 631–654. Analysis of fluid-structure interactions using a time-marching technique.
17. R. KING, M. J. PROSSER and D. J. JOHNS 1973 *Journal of Sound and Vibration* **29**, 169–188. On vortex excitation of model piles in water.
18. T. KITAGAWA, Y. FUJINO and K. KIMURA 1999 *Journal of Fluids and Structures* **13**, 499–518. Effects of free-end condition on end-cell-induced vibration.
19. R. LANDL 1975 *Journal of Sound and Vibration* **42**, 219–234. A mathematical model for vortex-excited vibrations of bluff bodies.
20. J.-C. LIN and D. ROCKWELL 1999 *Journal of Fluid Mechanics* **389**, 1–26. Horizontal oscillations of a cylinder beneath a free surface: vortex formation and loading.
21. Q. S. LU, C. W. S. TO and Z. S. JIN 1996 *Journal of Sound and Vibration* **190**, 791–820. Weak and strong interactions in vortex-induced resonant vibrations of cylindrical structures.
22. K. NAKAGAWA, K. KISHIDA and K. IGARASHI 1998 *Journal of Fluids and Structures* **12**, 759–777. Vortex-induced oscillation and lift of yawed circular cylinders in cross-flow.
23. T. SARPKAYA 1978 *Journal of the Waterway*, *Port*, *Coastal*, *and Ocean Division*, *Proceedings of the American Society of Civil Engineers* **104**, 275–290. Fluid forces on oscillating cylinders.
24. T. SARPKAYA 1995 *Journal of Offshore Mechanics and Arctic Engineering* **117**, 232–238. Hydrodynamic damping, flow-induced oscillations, and biharmonic response.
25. I. A. SIBETHEROS, R. W. MIKSAD, A.-V. VENTRE and K. F. LAMBRAKOS 1994 *Proceedings of the 4th International Offshore and Polar Engineering Conference*, *Osaka*, *Japan*, 10–15 *April* 406–412. Flow mapping of the reversing vortex wake of a cylinder in planar harmonic flow.
26. R. A. SKOP and S. BALASUBMRAMANIAN 1995 *Proceedings of the 5th International Offshore and Polar Engineering Conference*, *The Hague*, *The Netherlands*, 11–16 *June*, 578–581. A nonlinear oscillator model for vortex shedding from a forced cylinder. Part 1: uniform flow and model parameters.
27. R. A. SKOP and S. BALASUBMRAMANIAN 1995 *Proceedings of the Fifth International Offshore and Polar Engineering Conference*, *The Hague*, *The Netherlands*, 11–16 *June*, 582–586. A nonlinear oscillator model for vortex shedding from a forced cylinder. Part 2: shear flow and axial diffusion.
28. R. A. SKOP and S. BALASUBMRAMANIAN 1997 *Journal of Fluids and Structures* **11**, 395–412. A new twist on an old model for vortex-excited vibrations.
29. A. USCILOWSKA and J. A. KOLODZIEJ 1998 *Journal of Sound and Vibration* **216**, 147–157. Free vibration of an immersed column carrying a tip mass.
30. C. Y. ZHOU, R. M. C. SO and K. LAM 1999 *Journal of Fluids and Structures* **13**, 165–189. Vortex-induced vibrations of an elastic circular cylinder.
31. S. ZHU, Y. CAI and S. S. CHEN 1995 *Journal of Engineering Mechanics* **121**, 1003–1015. Experimental fluid-force coefficients for wake-induced cylinder vibration.
32. D. B. MCIVER 1973 *Journal of Engineering Mathematics* **7**, 249–261. Hamilton's principle for systems of changing mass.
33. C. LANCZOS 1970 *The Variational Principles of Mechanics*, 119–124. Dover: New York, fourth edition.
34. P. SHAH, P. ATSAVAPRANEE, T. Y. HSU, T. WEI and J. MCHUGH 1999 *Journal of Fluid Mechanics* **387**, 151. Turbulent transport in the core of a trailing delta wing vortex.

35. P. SHAH, P. ATSAVAPRANEE, T. WEI and J. MCHUGH 1999 *TAPPI Journal* **82**. The role of turbulent elongational stresses on deflocculation in paper sheet formation (in press).
36. T. Y. HSU, L. M. GREGA, T. WEI and R. I. LEIGHTON 2000 *Journal of Fluid Mechanics*. Kinetic energy transport in a corner formed by a solid wall and a free surface (in review).
37. P. ATSAVAPRANEE, A. VOORHEES, H. BENAROYA and T. WEI 2000 *Journal of Fluid Mechanics*. Lock-in regimes and vortex shedding modes on a cantilevered cylinder (in review).
38. G. B. SMITH 1992 *M. S. Thesis, Rutgers University*. Turbulent cascade to small scales during the off-axis collision of two vortex rings.
39. L. M. GREGA, T. WEI, R. I. LEIGHTON and J. C. NEVES 1995 *Journal of Fluid Mechanics* **294**, 17. Turbulent mixed-boundary flow in a corner formed by a solid wall and a free surface.
40. P. DONG, T. Y. HSU, P. ATSAVAPRANEE, and T. WEI 1999 *Experiments in Fluids* Digital particle image accelerometry (in print).
41. T. Y. HSU 1999 *M. S. Thesis, Rutgers University*. Turbulent transport in the mixed boundary corner formed by flow along a solid wall close to a free surface.
42. C. E. WILLERT and M. GHARIB 1991 *Experiments in Fluids* **10**, 181. Digital particle image velocimetry.
43. M. F. UNAL, J. C. LIN and D. O. ROCKWELL 1997 *Journal of Fluids and Structures* **11**, 965. Force prediction by PIV imaging: a momentum-based approach.